International Journal of Solids and Structures 176–177 (2019) 150–172

Contents lists available at ScienceDirect

International Journal of Solids and Structures

journal homepage: www.elsevier.com/locate/ijsolstr

Analysis of beam cross section response accounting for large strains and plasticity

Marco Morandini

Politecnico di Milano, Dipartimento di Scienze e Tecnologie Aerospaziali, via La Masa 34, Milano 20156, Italy

ARTICLE INFO

Article history:
Received 25 October 2018
Revised 4 May 2019
Accepted 15 May 2019
Available online 20 May 2019

Keywords:
Beam
Cross section
Nonlinear
Plasticity
Taylor expansion

ABSTRACT

The nonlinear response of straight, constant cross section of beams is investigated by means of a semi-analytical approach. The three dimensional displacement field is approximated, for a given cross section, using a FE element discretization on the section combined with a Taylor expansion in the beam axial direction. This allows to compute the beam cross section deformation as a function of the stress resultant and moment resultant, without the need to solve a three dimensional model, still allowing to account for complex three-dimensional constitutive laws.

1. Introduction

The behavior of slender structures is often approximated by means of so-called beam models. That is, the response of a solid slender structure of volume V, for which the deformed configuration is defined by the position field $\boldsymbol{x}'$ of its material points, is approximated by describing its configuration with a finite number of internal degrees of freedom; most often, but not necessarily, these degrees of freedom are the deformed position $\boldsymbol{x}'$ of the points on a reference line, and the parameters defining the deformed cross section orientation $\boldsymbol{\alpha}' \in \mathrm{SO}(3)$, an orthogonal tensor. In a nutshell, one ends up replacing the model of a solid with the model of a line equipped with some internal structure, be it the orientation of the beam cross section, as in Fig. 1, or the orientation enhanced with some additional parameters, such as in Vlasov-like models. The model reduction is obtained either axiomatically, i.e. by postulating the existence of a polar one-dimensional continuum (see e.g. Pietraszkiewicz and Eremeyev, 2009; Cardona and Geradin, 1988; Merlini and Morandini, 2013), or by projecting the three dimensional equilibrium equations onto a suitably-chosen set of cross section deformation modes. The first choice requires the definition of a constitutive law linking the generalized deformation measures of the reduced model to their work-conjugated internal actions; the second choice cannot easily be pursued without choosing beforehand the cross section deformation modes, and thus implicitly defining the generalized constitutive equation that would be needed for the first axiomatic approach.

Whatever choice is taken to reduce the problem dimensionality, the resulting beam model should match as much as possible the deformation energy of the solid. This is accomplished by a proper choice of the beam deformation modes. The simplest choice is to assume that the cross section do translate without any warping and change of dimension; this model, although well known, and often used by commercial finite element codes, is bound to the assumption that the only component of normal stress is the axial one, $\boldsymbol{S}_{zz}$, so that one can assume that $\boldsymbol{S}_{zz} = E\boldsymbol{\epsilon}_{zz}$, with E the Young modulus. This kinematic approximation is acceptable only for homogeneous cross sections. More advanced approaches, explicitly accounting for cross section warping, do compute the six de Saint–Venant's polynomial solutions, i.e. the six polynomial solutions for axial force, shear-bending along the two transverse directions, constant torsion and simple bending along the two transverse directions. The ensuing six displacement fields are used to perform the dimensional reduction. Giavotto et al. (1983) were perhaps the first authors to develop a robust and general numerical procedure that allows to compute the six polynomial solutions of an arbitrary cross section. After that work countless papers were written about the characterization of beam cross section, mostly following Giavotto et al. (1983) or Berdichevsky (1981), see also Hodges (2006); a slightly different approach was adopted in Morandini et al. (2010) and later on in Han and Bauchau (2015a), both based on an Hamiltonian setting (cfr. Mielke, 1991; Druz et al., 1996; Zubov, 2006; Romanova and Ustinov, 2008). When dealing with beams loaded by distributed

E-mail address: marco.morandini@polimi.it

https://doi.org/10.1016/j.ijsolstr.2019.05.014
0020-7683/

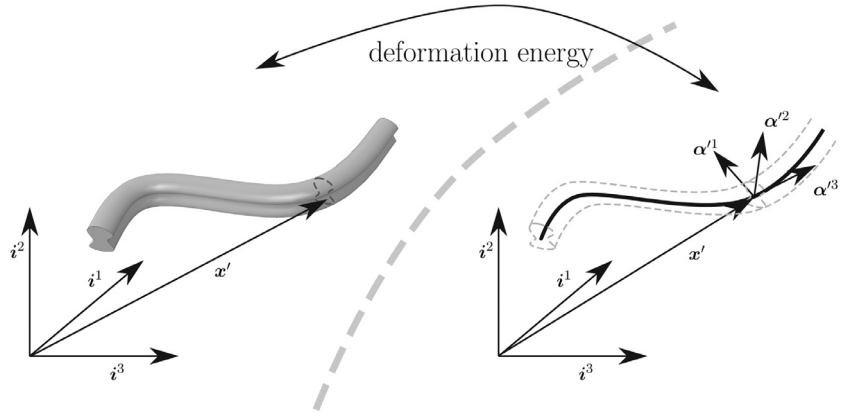

Fig. 1. Beam idealization.

forces the Taylor expansion solution for non homogeneous loaded beams proposed by Ieşan (1976) is worth mentioning, see also Ieşan (2008). A review encompassing many of the published papers can be found in Chakravarty (2011). Notable extensions are the application to curved beams (Borri et al., 1992; Cesnik, 1994) and to periodic cross sections (Han and Bauchau, 2016). Additional internal degrees of freedoms can further be introduced, helping describing self-equilibrated decaying solutions, that may be important especially when dealing with open thin-walled cross sections, see e.g. Garcea et al. (2016) and references therein, Ferradi et al. (2016) and, for plasticity, Corre et al. (2018).

The variational asymptotic method is based on Berdichevsky's work (e.g. Berdichevsky, 1981) and was developed by Hodges and his co-workers (see e.g. Hodges, 2006 and references therein). It naturally leads to the characterization of the four cross section deformation modes that are not function of the cross section position along the beam axis, namely axial force, torsion, and constant bending along the two transverse directions. The variational asymptotic method does not easily allow to study what happens when the shear deformation is different from zero. It is nonetheless possible to perform a second-order approximation and compute shear-induced deformations as well, see e.g. Popescu and Hodges (2000). The procedure proposed to account for shear deformation within the variationally asymptotic method is not straightforward, to the point that a small theoretical error, unnoticed for years, was discovered only recently by Yu et al. (2012); only after fixing that error the results obtained by the variationally asymptotic code were shown to be equal to those obtained by following Giavotto et al. (1983).

Most of the work available in the literature cited so far is limited to small cross section strain. This does not imply, however, that the beam model needs to be limited to small displacements and rotations: the section characterizations is performed once for all in a co-rotational framework, usually assuming a Green-elastic material. The use of Biot-like work-conjugated beam strain and internal action measures allows to correctly account for geometric stiffness contributions within the beam model. As a matter of fact it is standard practice in the multibody community to simulate the dynamics of rotating helicopter blades using the constitutive laws obtained using the above mentioned constitutive approaches. Few beam cross section characterization papers explicitly deal with nonlinear beam behavior, but are either limited to small-strain and large-displacement problems (Han and Bauchau, 2014), to small section warping (Borri and Merlini, 1986), or to known section normal stress field, computed from the linear solution (Merlini, 1988).

The variationally asymptotic method has been recently extended to the nonlinear characterization of beam cross sections by Jiang and Yu (2015). Their work is limited to a first-order asymptotic expansion. In other words, it can deal only with constant axial force, torsion and bending. Although the examples presented by Jiang and Yu (2015) deal only with tension and torsion their formulation leads to correct results for constant bending too. An extension to shear-loaded beams has been published by Jiang et al. (2018), but with a formulation that is limited to small strains.

Some recent papers deals with cross section elasto-plastic behavior of thin-walled beams; almost all of them, however, do assume from the beginning a given cross section deformation field (Rigobello et al., 2013) and/or that the only component of normal stress is the axial one, $\boldsymbol{S}_{zz}$ (Rezaiee-Pajand and Gharaei-Moghaddam, 2015; Chiorean, 2017). These assumptions are well warranted for thin-walled homogeneous beams, but could lead to wrong results with non-homogeneous cross sections. Specific approaches are also viable for particular geometries like concrete steel tubes (Wang et al., 2014).

The literature lacks a general beam cross section characterization method that can deal with arbitrary nonlinear constitutive laws and account, at the same time, for variable warping fields and transverse shear.

This paper is an attempt to provide a method to approximate the nonlinear response of an arbitrary beam cross section, while accounting for material non-linearities. The degree of the approximation can be chosen arbitrarily. The proposed approach, although general, has a clear limitation, since it approximates the beam response along the axis with a polynomial expansion that is computed as a function of the given beam internal actions only. As such, it cannot account for local cross section instabilities, for necking, or for local effects due to concentrated loads and/or constraints. It is clear that, in order to account for these phenomena one needs to solve the global beam elastic problem by means of a beam model enriched with carefully chosen warping functions, that would be work-conjugated to higher order moments of the cross section stress vector. The proposed approach is thus not suited for studying thin-walled cross section beams undergoing local instabilities. Nor it can be used, without modifications, to asses the actual load-carrying capacity of any given beam if the maximum of the internal actions is reached near a constraint or near to the point of application of a concentrated load.

2. Beam section kinematics

Let $\Omega = A \times \mathbb{R}$ be a right cylindrical beam, where A is the beam cross section. The beam axis is parallel to the z coordinate. The position in the reference and deformed configuration are $\boldsymbol{x}$ and $\boldsymbol{x}'$. The deformation gradient $\boldsymbol{F} = \mathrm{grad}(\boldsymbol{x}')$ can be decomposed in two terms, the first on the section plane, and the second given by its

vector component along the beam axis,

$$\boldsymbol{F} = \mathrm{grad}_S(\boldsymbol{x}') + \boldsymbol{x}'_{,z} \otimes \boldsymbol{i}^3, \tag{1}$$

where $\mathrm{grad}_S(\boldsymbol{x}') = \boldsymbol{x}'_{,x} \otimes \boldsymbol{i}^1 + \boldsymbol{x}'_{,y} \otimes \boldsymbol{i}^2$ and $\boldsymbol{x}'_{,x}$, $\boldsymbol{x}'_{,y}$ and $\boldsymbol{x}'_{,z}$ stand for the partial derivative of $\boldsymbol{x}'$ with respect to the coordinate x, y, z, respectively. Unit vectors $\boldsymbol{i}^1$, $\boldsymbol{i}^2$ and $\boldsymbol{i}^3$ are aligned with the chosen orthogonal reference system, with $\boldsymbol{i}^3$ parallel to the beam axis. The Green-Lagrange strain tensor is equal to

$$\boldsymbol{\epsilon} = \frac{1}{2}\left(\boldsymbol{F}^T\boldsymbol{F} - \boldsymbol{I}\right).$$

3. Virtual work principle

The virtual internal work reads

$$\begin{aligned}\delta\mathcal{L}_i &= \int_V \delta\boldsymbol{\epsilon} : \boldsymbol{S}\mathrm{d}V = \int_V \delta\boldsymbol{F} : \hat{\boldsymbol{S}}\mathrm{d}V \\ &= \int_V \delta\mathrm{grad}_S(\boldsymbol{x}') : \hat{\boldsymbol{S}}\mathrm{d}V + \int_V \delta\boldsymbol{x}'_{,z} \otimes \boldsymbol{i} : \hat{\boldsymbol{S}}\mathrm{d}V\end{aligned} \tag{2}$$

with $\boldsymbol{\epsilon} = \frac{1}{2}\left(\boldsymbol{F}^T\boldsymbol{F} - \boldsymbol{I}\right)$ the Green-Lagrange strain tensor, $\hat{\boldsymbol{S}}$ and $\boldsymbol{S}$ the first and second Piola–Kirchhoff stress tensors, respectively. The second term of Eq. (2) can be reworked as

$$\begin{aligned}\int_V \delta\boldsymbol{x}'_{,z} \otimes \boldsymbol{i}^3 : \hat{\boldsymbol{S}}\mathrm{d}V &= \int_V \delta\boldsymbol{x}'_{,z} \cdot \hat{\boldsymbol{S}} \cdot \boldsymbol{i}^3\mathrm{d}V = \int_V \delta\boldsymbol{x}'_{,z} \cdot \hat{\boldsymbol{S}} \cdot \bar{\boldsymbol{n}}\mathrm{d}V \\ &= \int_L\int_A \delta\boldsymbol{x}'_{,z} \cdot \hat{\boldsymbol{S}} \cdot \bar{\boldsymbol{n}}\mathrm{d}A\mathrm{d}z,\end{aligned} \tag{3}$$

with $\bar{\boldsymbol{n}} \equiv \boldsymbol{i}^3$. Eq. (3) can be integrated by part as

$$\begin{aligned}\int_L\int_A \delta\boldsymbol{x}'_{,z} \cdot \hat{\boldsymbol{S}} \cdot \bar{\boldsymbol{n}}\mathrm{d}A\mathrm{d}z &= \int_L \left(\frac{\mathrm{d}}{\mathrm{d}z}\int_A \delta\boldsymbol{x}' \cdot \hat{\boldsymbol{S}} \cdot \bar{\boldsymbol{n}}\mathrm{d}A\right)\mathrm{d}z - \int_L\int_A \delta\boldsymbol{x}' \cdot \hat{\boldsymbol{S}}_{,z} \cdot \bar{\boldsymbol{n}}\mathrm{d}A\mathrm{d}z \\ &= \left[\int_A \delta\boldsymbol{x}' \cdot \hat{\boldsymbol{S}} \cdot \bar{\boldsymbol{n}}\mathrm{d}A\right]_0^L - \int_L\int_A \delta\boldsymbol{x}' \cdot \hat{\boldsymbol{S}}_{,z} \cdot \bar{\boldsymbol{n}}\mathrm{d}A\mathrm{d}z \\ &= \left[\int_A \delta\boldsymbol{x}' \cdot \hat{\boldsymbol{S}} \cdot \boldsymbol{n}\mathrm{d}A\right]_L + \left[\int_A \delta\boldsymbol{x}' \cdot \hat{\boldsymbol{S}} \cdot \boldsymbol{n}\mathrm{d}A\right]_0 + \\ &\quad - \int_L\int_A \delta\boldsymbol{x}' \cdot \hat{\boldsymbol{S}}_{,z} \cdot \bar{\boldsymbol{n}}\mathrm{d}A\mathrm{d}z,\end{aligned} \tag{4}$$

where $\boldsymbol{n}$ is the outward-pointing normal of the beam (with reference to Fig. 2, $\boldsymbol{n} = \bar{\boldsymbol{n}}$ for $z = L$ and $\boldsymbol{n} = -\bar{\boldsymbol{n}}$ for $z = 0$). The internal work is therefore the sum of three main contributions: a boundary term and two integral terms, the first containing the derivatives along the beam axis, the second the derivatives with respect to the section plane. The formulation is here limited to end loads, neglecting distributed loads along the beam axis. The virtual work of the applied external forces is thus equal to

$$\delta\mathcal{L}_e = \int_A \delta\boldsymbol{x}'(L) \cdot \boldsymbol{f}(L)\mathrm{d}A + \int_A \delta\boldsymbol{x}'(0) \cdot \boldsymbol{f}(0)\mathrm{d}A. \tag{5}$$

The equilibrium is therefore satisfied if

$$\begin{aligned}&-\int_L\int_A \delta\boldsymbol{x}' \otimes \bar{\boldsymbol{n}} : \hat{\boldsymbol{S}}_{,z}\mathrm{d}A\mathrm{d}z + \int_L\int_A \delta\mathrm{grad}_S(\boldsymbol{x}') : \hat{\boldsymbol{S}}\mathrm{d}A\mathrm{d}z \\ &+\left[\int_A \delta\boldsymbol{x}' \cdot \left(\hat{\boldsymbol{S}} \cdot \boldsymbol{n} - \boldsymbol{f}\right)\mathrm{d}A\right]_L + \left[\int_A \delta\boldsymbol{x}' \cdot \left(\hat{\boldsymbol{S}} \cdot \boldsymbol{n} - \boldsymbol{f}\right)\mathrm{d}A\right]_0 = 0.\end{aligned} \tag{6}$$

The first two integrals constitute the global equilibrium equations, while the last two integrals represent the natural boundary conditions at the end of the beam, $\hat{\boldsymbol{S}} \cdot \boldsymbol{n} = \boldsymbol{f}$. The equilibrium equations along the beam is satisfied if

$$-\int_A \delta\boldsymbol{x}' \otimes \bar{\boldsymbol{n}} : \hat{\boldsymbol{S}}_{,z}\mathrm{d}A + \int_A \delta\mathrm{grad}_S(\boldsymbol{x}') : \hat{\boldsymbol{S}}\mathrm{d}A = 0 \tag{7}$$

along the beam.

The structure of Eq. (7) solutions is well known: six rigid-body displacements of the whole beam, the six so-called de Saint–Venant's solutions, and self-equilibrated displacement fields that, for small-strain linear elasticity, are exponentially decaying with respect to z. Note also that for non-linear elasticity one can, in principle, track the evolution of the exponential terms wrt. a load parameter in order to assess the occurrence of local buckling, see e.g. Merlini (1988). For small-strain linear elasticity the rigid-body and the de Saint–Venant's displacement fields are polynomial with respect to z, with the quadratic and cubic terms accounting for bending and transverse shear, respectively; knowledge of the polynomial solutions allows to compute the 6×6 beam stiffness matrix and to recover the three-dimensional stress field as a function of the beam internal actions.

Seeking a closed-form solution of Eq. (7) along the beam without assuming small strains and/or small section warping can be a tough problem to solve, especially with non-linear material models. It is however possible to locally approximate the solution $\boldsymbol{x}'$ at $z = 0$ without limiting the strain magnitude and thus to seek a displacement field that locally approximates the three-dimensional solution. To this end, Eq. (7) is enforced at $z = 0$ only, and no attempt is made to actually solve the differential equation along the whole beam, thus neglecting whatever boundary conditions could be imposed at the two beam extremities. This is clearly not sufficient to approximate the solution along the beam. To get a better approximation, still solving a problem only at $z = 0$, one can consider both Eq. (7) and it subsequent derivatives wrt. z. The first derivative would read

$$\begin{aligned}&-\int_A \delta\boldsymbol{x}'_{,z} \otimes \bar{\boldsymbol{n}} : \hat{\boldsymbol{S}}_{,z}\mathrm{d}A - \int_A \delta\boldsymbol{x}' \otimes \bar{\boldsymbol{n}} : \hat{\boldsymbol{S}}_{,zz}\mathrm{d}A \\ &+\int_A \delta\left(\mathrm{grad}_S\boldsymbol{x}'\right)_{,z} : \hat{\boldsymbol{S}}\mathrm{d}A + \int_A \delta\mathrm{grad}_S\boldsymbol{x}' : \hat{\boldsymbol{S}}_{,z}\mathrm{d}A = 0,\end{aligned} \tag{8}$$

where the derivative $\delta\boldsymbol{x}'_{,z}$, always evaluated at $z = 0$, appears. Writing the expression of any subsequent derivative is straightforward.

The sought displacement field $\boldsymbol{u}$ is approximated around $z = 0$ as

$$\boldsymbol{u}(x, y, z) \approx \sum_{i=0}^{N} \frac{1}{i!}\boldsymbol{u}_i(x, y)z^i, \tag{9}$$

where the unknown field $\boldsymbol{u}_i(x, y)$, a function of the cross section position only, is the i-th displacement derivative of field $\boldsymbol{u}(x, y, z)$ wrt. z evaluated at $z = 0$. For example, one can adopt a linear approximation $\boldsymbol{u} \approx \boldsymbol{u}_0 + \boldsymbol{u}_1 z$, a quadratic one, $\boldsymbol{u} \approx \boldsymbol{u}_0 + \boldsymbol{u}_1 z + \frac{1}{2}\boldsymbol{u}_2 z^2$, or even a cubic one, $\boldsymbol{u} \approx \boldsymbol{u}_0 + \boldsymbol{u}_1 z + \frac{1}{2}\boldsymbol{u}_2 z^2 + \frac{1}{6}\boldsymbol{u}_3 z^3$. A Galerkin method is adopted to solve the problem, with the test function defined by $\delta\boldsymbol{u} = \sum_{i=0}^{N} \frac{1}{i!}\delta\boldsymbol{u}_i(x, y)z^i$, and $\delta\boldsymbol{u}_i(x, y)$ resorting to the same cross-section approximation adopted for the unknown fields $\boldsymbol{u}_i$.

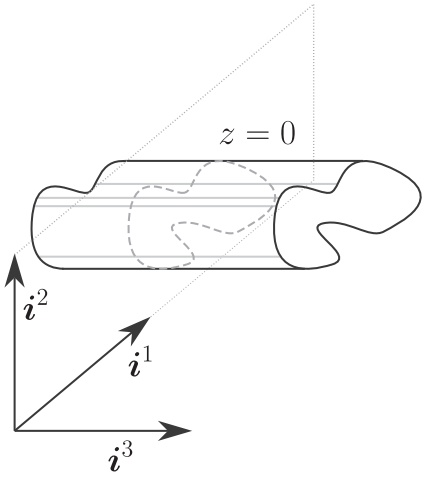

Fig. 2. Local reference frame on a beam slice.

Eq. (7), evaluated at $z = 0$, does not allow to compute, at the same time, all the unknown fields $\boldsymbol{u}_i$. Rather, it suffices to compute only the 0-th order term, $\boldsymbol{u}_0$. This should not be a surprise, since the test function $\delta\boldsymbol{x}'$ at $z = 0$ is nothing but $\delta\boldsymbol{u}_0$ alone. In order to compute both $\boldsymbol{u}_0$ and $\boldsymbol{u}_1$ one needs to account, at the same time, for Eq. (7) and for Eq. (8), where the derivative $\delta\boldsymbol{x}'_{,z}$ evaluated at $z = 0$ appears. Note that this derivative is equal, for the chosen approximation Eq. (9), to $\delta\boldsymbol{u}_1$. Each and every additional term added to Eq. (9) requires, in turn, an additional derivative of Eq. (7), with a corresponding new derivative $\delta(\partial^i\boldsymbol{x}'/\partial z^i)$ that, after applying the approximation Eq. (9), corresponds to $\delta\boldsymbol{u}_i$.

No boundary conditions has been considered so far. To close the problem, the set of Eqs. (7) and of its derivatives (i.e. Eqs. (7) and (8) when $N = 1$ in Eq. (9)) can be complemented by six equations that impose the sought value of the stress resultant $\boldsymbol{t}$ and moment resultant $\boldsymbol{m}$ at $z = 0$ together with six additional constraints for the beam rigid body motions. The sought vectors $\boldsymbol{t}$ and $\boldsymbol{m}$ are imposed to be equal to the resultant and moment resultant, over the cross-section, of the normal stress vector $\hat{\boldsymbol{S}} \cdot \boldsymbol{n}$, i.e.

$$\begin{aligned} &\int_A \hat{\boldsymbol{S}} \cdot \overline{\boldsymbol{n}} \mathrm{d}A = \boldsymbol{t}, \\ &\int_A \boldsymbol{x}' \times \hat{\boldsymbol{S}} \cdot \overline{\boldsymbol{n}} \mathrm{d}A = \boldsymbol{m}. \end{aligned} \tag{10}$$

Eqs. (10) are enforced by using two Lagrange multiplier vectors, $\boldsymbol{\lambda}_1$ and $\boldsymbol{\lambda}_2$. Note that Eqs. (10) involves only the first Piola–Kirchhoff stress tensor $\hat{\boldsymbol{S}}$ evaluated at $z = 0$; they thus depend explicitly only on the deformation gradient $\boldsymbol{F}$ evaluated at $z = 0$, i.e. on the first two terms of the approximation, $\boldsymbol{u}_0$ and $\boldsymbol{u}_1$. The rigid body motion constraints are imposed by forcing to zero the projection of the cross section displacement $\boldsymbol{u}$ at $z = 0$ (i.e. $\boldsymbol{u}_0$) onto the corresponding rigid body displacement fields; that is,

$$\begin{aligned} &\int_A \boldsymbol{u}_0 \mathrm{d}A = \boldsymbol{0}, \\ &\int_A \boldsymbol{x} \times \boldsymbol{u}_0 \mathrm{d}A = \boldsymbol{0}. \end{aligned} \tag{11}$$

Eqs. (11) are imposed by using two additional Lagrange multiplier vectors, $\boldsymbol{\lambda}_3$ and $\boldsymbol{\lambda}_4$.

For a linear approximation, $N = 1$, the whole set of nonlinear Eqs. (7), (8), (10) and (11) has $\delta\boldsymbol{u}_0$, $\delta\boldsymbol{u}_1$ and $\delta\boldsymbol{\lambda}_j$, with $j \in [1, 4]$, as independent test functions, and $\boldsymbol{u}_0$, $\boldsymbol{u}_1$ and $\boldsymbol{\lambda}_j$ as unknowns; this set of equations can be solved as a function of the sought internal actions $\boldsymbol{t}$ and $\boldsymbol{m}$. No additional constraints, besides those of Eqs. (10) and (11), are required for $N \geq 2$. This allows to compute the strain and stress distribution at any given beam section as a function of the internal actions, regardless of the constitutive law at hand, be it Cauchy-elastic, hyperelastic, or elasto-plastic.

A drawback of the proposed approach is that it needs explicit expressions for $N + 1$ derivatives of the first Piola–Kichhoff stress tensor $\hat{\boldsymbol{S}}$ with respect to z. Limiting again the approximation to the first order, $N = 1$, this means $\hat{\boldsymbol{S}}_{,z}$ and $\hat{\boldsymbol{S}}_{,zz}$. This is not a big issue for hyperelastic materials, and complicates the matter only slightly; however, it brings significant additional complexity for elasto-plastic materials: one needs to compute the first and second derivatives of the plastic multiplier in order to compute $\hat{\boldsymbol{S}}_{,z}$ and $\hat{\boldsymbol{S}}_{,zz}$, as detailed in Appendix A for a simple elasto-plastic constitutive laws.

Standard Lagrange elements are used to approximate $\boldsymbol{u}_i$.

4. Validation

The proposed formulation is validated by comparing its results with those of three-dimensional models of the beam at hand. All the examples are made, without loss of generality, for a $1\,\mathrm{m} \times 1\,\mathrm{m}$ square cross sections centered at the origin. The two-dimensional model is made using cubic triangles with a 10×10 subdivision of the cross section.

The three-dimensional model used for comparison has a length of 4 m. The same constraints used for the cross section analysis are applied to the three dimensional body; that is, the section at $z = 0$ m is constrained by the same Eqs. (11) defined for the two-dimensional formulation. This eases the comparison between the results of the three dimensional model and of the proposed formulation. The loads definition is a bit more tricky: the three dimensional solid needs to be loaded at the two beam extremities, far from the middle section at $z = 0$ m in order to damp out any local effect, in such a way that the middle section reacts with the sought internal actions $\boldsymbol{t}$ and $\boldsymbol{m}$. This allows to precisely control the internal action of the three dimensional model at $z = 0$ m. Details on how this is accomplished can be found in Appendix B.

The solid mesh is made using cubic tetrahedrons with a $10 \times 10 \times 20$ subdivision of the volume.

Both the three- and the two-dimensional models' equations are solved using Newton–Rhapson; the linearized equations, however, are rather ill-conditioned for the three-dimensional model, possibly because of the highly coupled and nonlinear additional equations enforcing both the middle cross section internal actions and the global equilibrium. Typical deformed shapes of the three-dimensional model are reported, without magnification of the

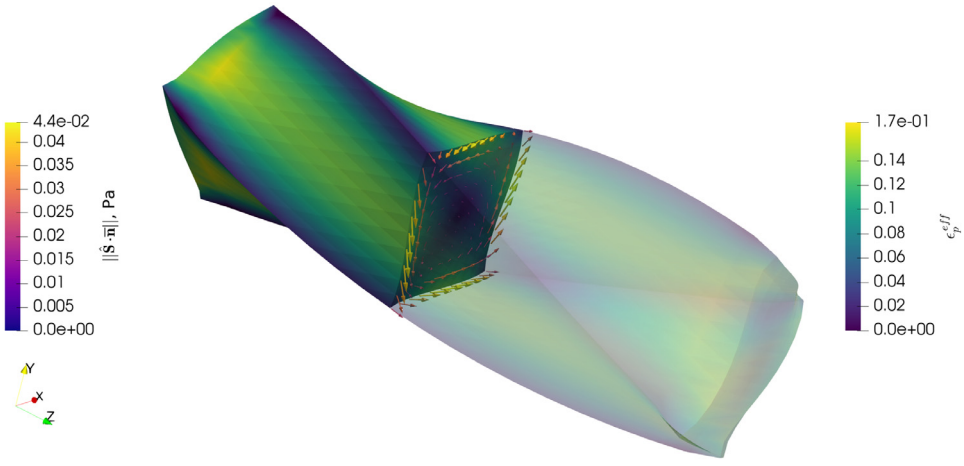

Fig. 3. Torsion of an elasto-plastic beam; ε_p^{eff} is the equivalent plastic strain.

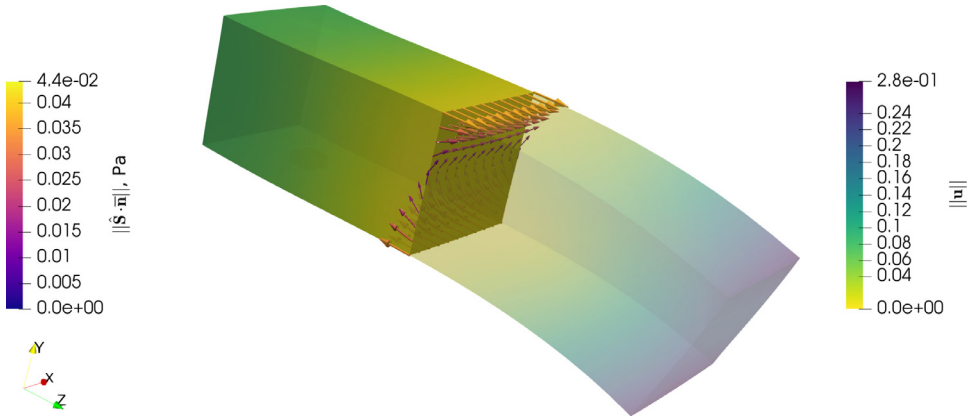

Fig. 4. Shear-bending of an elastic beam.

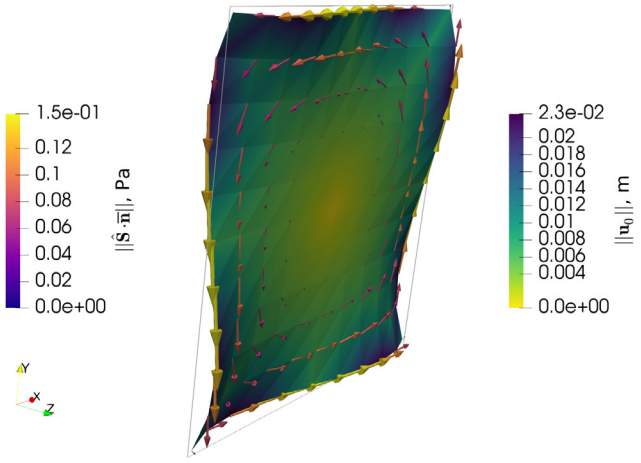

Fig. 5. Torsion of a Green-elastic beam: deformed configuration and normal stress vector $\hat{\boldsymbol{S}} \cdot \bar{\boldsymbol{n}}$, $m_z = 0.03\,\text{Nm}$.

displacements, in Figs. 3 and 4. Fig. 3 shows the torsion of an elasto-plastic beam, and Fig. 4 the combined shear-bending of an elastic beam; arrows in the cross section represents the first stress vector $\hat{\boldsymbol{S}} \cdot \bar{\boldsymbol{n}}$ projected onto linear Lagrange vector finite elements.

All the simulations are performed by leveraging the python interface of Dolfin (Logg and Wells, 2010; Logg et al., 2012b), a library developed within the FEniCS project (Alnæs et al., 2015; Logg et al., 2012a).

Standard third-order Lagrange elements are used for all the examples; the displacements are not magnified for plotting the deformed shapes.

All results are obtained, unless otherwise specified, by limiting the unknown displacement expansion Eq. 9 to a first order approximation, $N = 1$.

4.1. Torsion

The beam is made of an isotropic Green-elastic material, for which $\boldsymbol{S} = 2\mu\boldsymbol{\epsilon} + \lambda\boldsymbol{\epsilon} : \boldsymbol{I} \otimes \boldsymbol{I}$, with $\mu = E/(2(1+\nu))$ and $\lambda = E\nu/((1+\nu)(1-2\nu))$, where $E = 1\,\text{Pa}$ is the Young modulus and $\nu = 0.33$ is the Poisson coefficient. The sought moment is equal to $m_z = 0.03\,\text{Nm}$. Fig. 5 shows the cross section deformed shape together with the first stress vector $\hat{\boldsymbol{S}} \cdot \bar{\boldsymbol{n}}$ projected onto linear Lagrange vector finite elements. Fig. 6 compares the norm of the displacement difference between the three-dimensional solution and the proposed approach for $z = 0\,\text{m}$ (left figure) and $z = 0.2$ m (right figure), normalized with respect to the maximum displacement norm $||\boldsymbol{u}_{\text{FEM}}||_{\max} = 0.023$ m and $||\boldsymbol{u}_{\text{FEM}}||_{\max} = 0.083$ m, respectively; the displacement of the nearby section at $z = 0.2\,\text{m}$ are approximated, for the proposed approach, as $\boldsymbol{u} \approx \boldsymbol{u}_0 + 0.2\boldsymbol{u}_1$. Fig. 7 plots the relative difference for the cross sections stress vector norm $||\hat{\boldsymbol{S}} \cdot \bar{\boldsymbol{n}}||$, normalized with respect to its maximum value $||\hat{\boldsymbol{S}} \cdot \bar{\boldsymbol{n}}||_{\text{FEM max}} = 0.15\,\text{Pa}$.

4.1.1. Neo-Hookean material

Although not immediately evident from the previous results, the simulation is completely non linear, and can account for

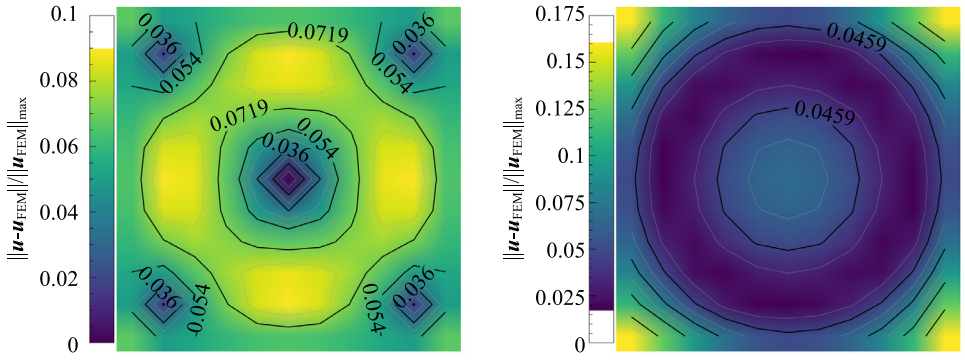

Fig. 6. Torsion of a Green-elastic beam: displacement relative difference, $m_z = 0.03\,\text{Nm}$; left: $z = 0$ m; right: $z = 0.2\,\text{m}$.

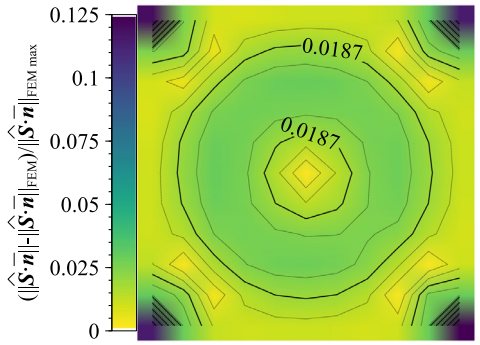

Fig. 7. Torsion of a Green-elastic beam: $||\hat{\boldsymbol{S}}\cdot\overline{\boldsymbol{n}}||$ relative difference, $m_z = 0.03\,\text{Nm}$, $z = 0$ m.

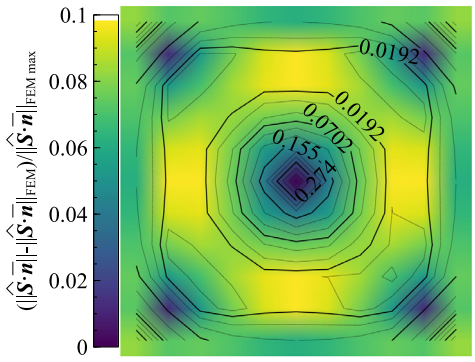

Fig. 10. Torsion of an elasto-plastic beam: $||\hat{\boldsymbol{S}}\cdot\overline{\boldsymbol{n}}||$ relative difference, $m_z = 0.009\,\text{Nm}$, $z = 0$ m.

nonlinear material behavior as well. Consider the same beam made with an isotropic Neo-Hookean material with internal energy per unit of reference volume $w = \frac{\mu}{2}(I_1 - 3) + \frac{K_0}{2}(J-1)^2$, where $\mu = E/(2(1+\nu))$, $\lambda = E\nu/((1+\nu)(1-2\nu))$, $K_0 = E/(3(1-2\nu))$, $J = \det(\boldsymbol{F})$, $I_1 = J^{-2/3}(\boldsymbol{F}^T\boldsymbol{F}) : \boldsymbol{I}$, $E = 1\,\text{Pa}$ and $\nu = 0.33$. To visually appreciate the difference with respect to the Green-elastic material the sought moment is equal to $m_z = 0.1\,\text{Nm}$, much higher than that of the previous example, to the point that the three-dimensional code hardly converges. Fig. 8 compares the cross section deformed shape $\boldsymbol{x} + \boldsymbol{u}_0$ obtained with the proposed approach and the two different materials, together with the first stress vector $\hat{\boldsymbol{S}}\cdot\overline{\boldsymbol{n}}$.

4.1.2. Elasto-plastic material

More interesting, elasto-plastic materials can be accounted for. The elasto-plastic material of Appendix A.1 is considered, with $\mathbb{E}$ the elastic tensor of a Green-elastic isotropic material, $E = 1\,\text{Pa}$ the elastic modulus, $\nu = 0.33$ the Poisson coefficient, $S_0 = 0.01\,\text{Pa}$ the yield stress, $H = E_t/(1 - E_t/E)$ the hardening parameter and $E_t = 0.3\,\text{Pa}$ the tangent elasto-plastic modulus. Since the beam undergoes significant plastic deformations its stiffness is reduced, and the results are computed for a moment $m_z = 0.009\,\text{Nm}$. Fig. 9 compares the norm of the displacement difference between the three-dimensional solution and the proposed approach for $z = 0\,\text{m}$ (left figure) and $z = 0.2$ m (right figure), normalized with respect to the maximum displacement norm $||\boldsymbol{u}_{\text{FEM}}||_{\max} = .021$ m and $||\boldsymbol{u}_{\text{FEM}}||_{\max} = .074$ m, respectively. Fig. 10 reports the relative difference for the cross sections stress vector norm $||\hat{\boldsymbol{S}}\cdot\overline{\boldsymbol{n}}||$, normalized with respect to its maximum value $||\hat{\boldsymbol{S}}\cdot\overline{\boldsymbol{n}}||_{\text{FEM max}} = 0.044\,\text{Pa}$; finally, Fig. 11 plots the relative equivalent plastic strain difference, normalized with respect to its maximum value $(\epsilon^{eff}_{p\,\text{FEM}})_{\max} = 0.14$. Since the plastic strain is null near the cross section torsional

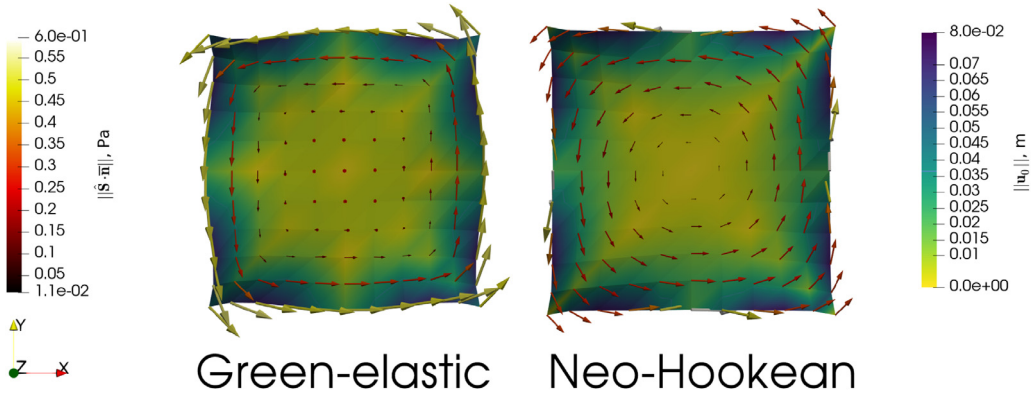

Fig. 8. Torsion of a Green-elastic beam: deformed configuration and normal stress vector $\hat{\boldsymbol{S}}\cdot\overline{\boldsymbol{n}}$, $m_z = 0.03\,\text{Nm}$, $z = 0$ m.

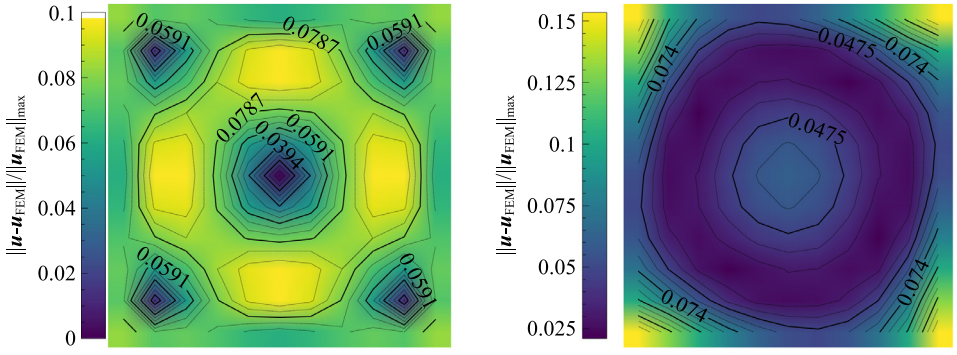

Fig. 9. Torsion of an elasto-plastic beam: displacement relative difference, $m_z = 0.009\,\text{Nm}$; left: $z = 0$ m; right: $z = 0.2\,\text{m}$.

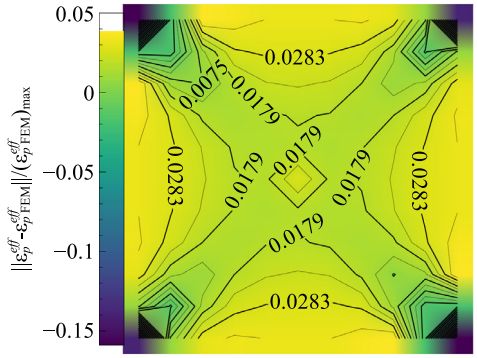

Fig. 11. Torsion of an elasto-plastic beam: equivalent plastic strain ϵ_p^{eff} relative difference, $m_z = 0.009\,\mathrm{Nm}$, $z = 0$ m.

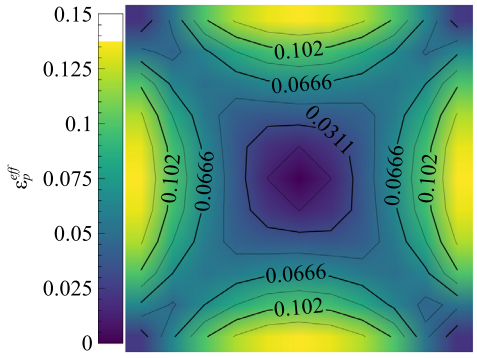

Fig. 12. Torsion of an elasto-plastic beam: equivalent plastic strain ϵ_p^{eff}, $m_z = 0.009\,\mathrm{Nm}$, $z = 0$ m.

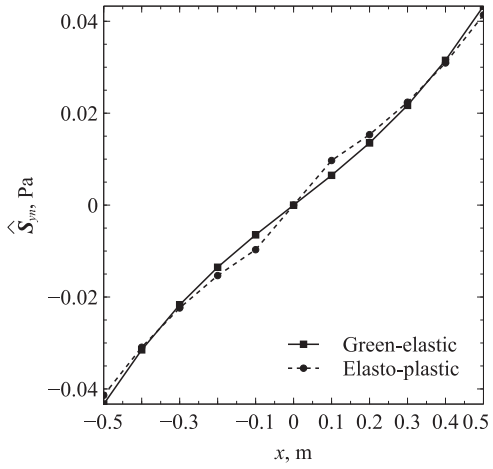

Fig. 13. Torsion of elastic and elasto-plastic beams: shear component $\hat{S}_{yn}$ plotted along $y = 0\,\mathrm{m}$, $m_z = 0.009\,\mathrm{Nm}$, $z = 0$ m.

center, as it should (cfr. also Fig. 12), the stress distribution is different from that of a beam made of an elastic material. This is clear from Fig. 13, that plots the shear component $\hat{S}_{yn}$ along the line $y = 0\,\mathrm{m}$ for the Green-elastic and the elasto-plastic beam under the moment $m_z = 0.009\,\mathrm{Nm}$.

4.1.3. Axial force stiffening

Since the beam section code is completely nonlinear it is possible to apply complex internal actions time histories and follow the cross section deformation throughout. For example, Fig. 14 shows the effect of first applying a torsional moment $m_z = 0.06\,\mathrm{Nm}$ and then superposing an axial force $t_z = 0.6\,\mathrm{N}$ onto the Green-elastic beam of Section 4.1; the axial force stiffening effect is correctly accounted for in the simulation, so that the cross section at $z = 0.2\,\mathrm{m}$ sees a reduced rotation while moving along the beam axis. By projecting the in-plane components of $\boldsymbol{u}_1$ onto the rigid mode rotation rate of the undeformed section, defined as a nonlinear function of the rotation angle derivative $\alpha_{,z}$ it is possible to compute the actual value of the rotation derivative $\alpha_{,z}$ and thus to compute the torsional compliance $a_{,z}/m_z$. Figs. 15 plot the torsional compliance as a function of the applied moment (left, with null axial force t_z) and of the axial force resultant t_z (right, with constant applied moment $m_z = 0.06\,\mathrm{Nm}$).

4.2. Shear-bending

The test cases of Section 4.1 are characterized by a deformation field that is constant with respect to the beam axis. This is not the case when the internal actions have any non zero force component in the cross section plane, since the bending moment varies linearly. The three-dimensional case of Fig. 4 allows to verify the soundness of the proposed approach whenever the beam deformation varies due to transverse shear. The Green-elastic beam with $E = 1\,\mathrm{Pa}$ and $\nu = 0.33$ is loaded at $z = 0\,\mathrm{m}$ with $t_y = 0.01\,\mathrm{N}$ and $m_x = 0.008\,\mathrm{Nm}$. Fig. 16 compares the displacement field at $z = 0\,\mathrm{m}$ and $z = 0.2\,\mathrm{m}$ with that of the three-dimensional model; the displacement difference is normalized with respect to the maximum displacement norm $||\boldsymbol{u}_{\mathrm{FEM}}||_{\max} = 0.0081$ m and $||\boldsymbol{u}_{\mathrm{FEM}}||_{\max} = 0.015$ m, respectively. The displacement difference appears to be more significant than that of the torsion cases, especially at the cross section corners. The relative difference for the cross sections stress vector $||\hat{\boldsymbol{S}} \cdot \overline{\boldsymbol{n}}||$, normalized with respect to the maximum value $||\hat{\boldsymbol{S}} \cdot \overline{\boldsymbol{n}}||_{\mathrm{FEM\ max}} = 0.051\,\mathrm{Pa}$ is less marked, as shown in Fig. 17.

Although the normal stress difference obtained with the linear approximation could be judged acceptable, it is nonetheless clear that a linear approximation may not be the wisest choice for a problem that is known to have, in linear elasticity, a cubic displacement field wrt. z. Figs. 18 and 19 report the relative difference obtained by choosing a quadratic and cubic approximation for $\boldsymbol{u}$, respectively (i.e. $N = 2$ and $N = 3$ in Eq. (9), with additional unknown fields $\boldsymbol{u}_2$ and $\boldsymbol{u}_3$). It's clear that increasing the approximation order reduces the difference wrt. the three-dimensional solution. This, however, has a non-negligible cost, as one needs to add to the set of equations the second derivative of Eq. (7) for the quadratic approximation, and its second and third derivatives for the cubic approximations. This, in turn, brings the need to compute the third (quadratic approximation) and fourth (cubic approximation) derivatives of the normal stress vector, $\hat{\boldsymbol{S}}_{,zzz} \cdot \overline{\boldsymbol{n}}$ and $\hat{\boldsymbol{S}}_{,zzzz} \cdot \overline{\boldsymbol{n}}$, a rather tedious task. Fig. 20 plots the relative difference for the cross sections stress vector $||\hat{\boldsymbol{S}} \cdot \overline{\boldsymbol{n}}||$ obtained with the quadratic and cubic approximations.

The convergence error of the three-dimensional solution is large for this specific test case, likely because of the ill-conditioned set of integral constraints applied at the two beam extremities and at its center cross section. Fig. 21 shows the cross section deformed shape together with the first stress vector $\hat{\boldsymbol{S}} \cdot \overline{\boldsymbol{n}}$ computed for section internal actions equal to $t_y = 0.05\,\mathrm{N}$ and $m_x = 0.04\,\mathrm{Nm}$, values that are not reachable with the three-dimensional formulation.

4.2.1. Elasto-plastic bending

The same beam, but with the elasto-plastic constitutive law of Section 4.1.2 is subject to a bending moment $m_x = 0.005$ Nm. Three solutions are considered, obtained using the present formulation with a 50×50 mesh of linear elements and a quadratic approximation along the beam axis, a 3D finite element model

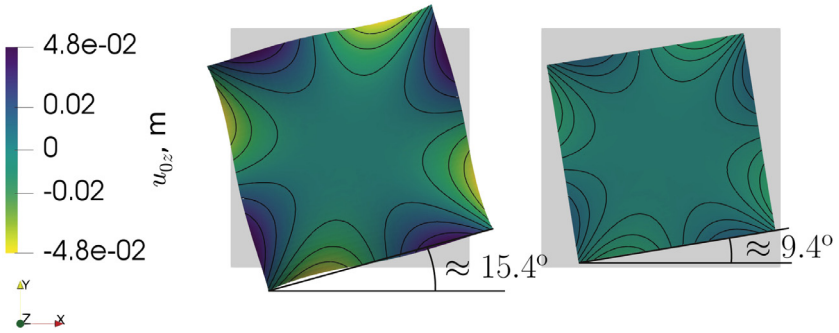

Fig. 14. Combined torsion and axial force of an elastic beam; left: deformed section at $z = 0.2$ m, torsion without traction, $m_z = 0.06$ Nm, $t_z = 0$ N; right: deformed section at $z = 0.2$ m, torsion and traction, $m_z = 0.06$ Nm, $t_z = 0.6$ N; undeformed sections in gray.

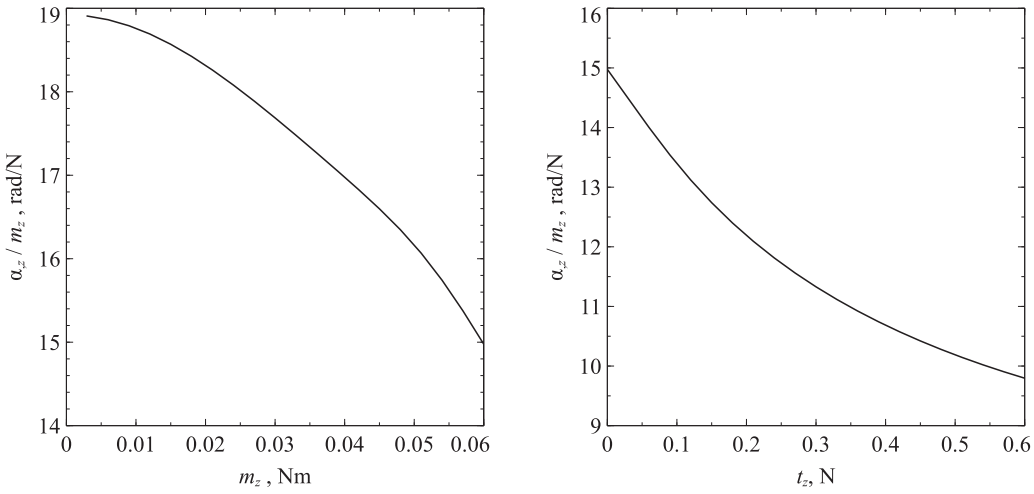

Fig. 15. Combined torsion and axial force of an elastic beam; left: α_z/m_z as a function of m_z, $t_z = 0$ N; right: α_z/m_z as a function of t_z, $m_z = 0.06$ Nm.

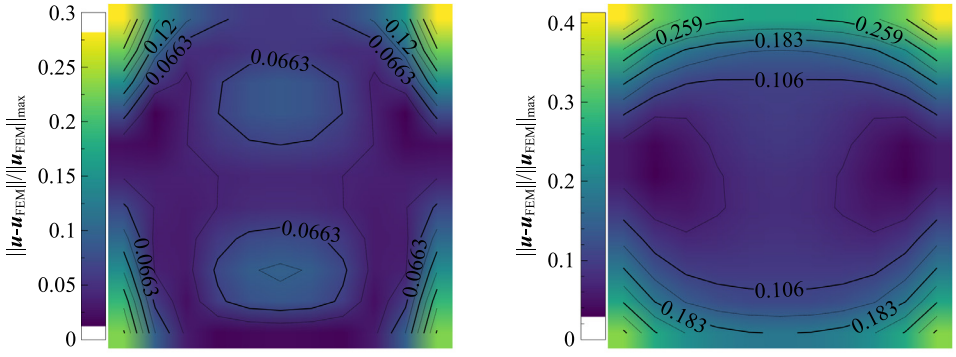

Fig. 16. Shear-bending of a Green-elastic beam: displacement relative difference, $t_y = 0.01$ N and $m_x = 0.008$ Nm; left: $z = 0$ m; right: $z = 0.2$ m.

with a $50 \times 50 \times 24$ mesh with linear elements and an approximate analytical solution where the axial strain is assumed to be linear with respect to y and a state of axial stress is assumed. Fig. 22 (left) compares the y position of the elastic zone boundary, while Fig. 22 (right) reports the bending moment m_x as a function of the estimated beam curvature. The agreement between the three formulations if fairly good for this simple test case. Fig. 23 reports the norm of $\hat{\boldsymbol{S}} \cdot \boldsymbol{i}^1$ and $\hat{\boldsymbol{S}} \cdot \boldsymbol{i}^2$ stress vectors, that are overlooked by the analytical axial stress approximation.

4.2.2. Elasto-plastic shear bending

Elasto-plastic shear bending can be accounted for as well. The material data are the same of Sections 4.1.2 and 4.2.1. The cross section internal actions are $t_y = 0.006$ N and $m_x = 0.0048$ Nm. The solid model has a reduced length of 2 m, since otherwise the bending moment at one of the two beam extremities could likely be too high. A 10×10 cubic elements mesh, with a cubic approximation along the beam axis, is adopted for the cross section analysis, while the three dimensional model is built with a $10 \times 10 \times 20$ cubic elements mesh. Fig. 24 compares the

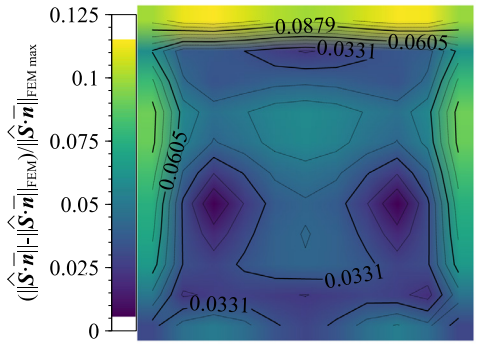

Fig. 17. Shear-bending of a Green-elastic beam: $||\hat{\boldsymbol{S}} \cdot \overline{\boldsymbol{n}}||$ relative difference, $t_y = 0.01$ N and $m_x = 0.008$ Nm.

displacement field at $z = 0$ m and $z = 0.2$ m with that of the three-dimensional model; the displacement difference is normalized with respect to the maximum displacement norm of $||\boldsymbol{u}_{\text{FEM}}||_{\max} = 0.014$ m and $||\boldsymbol{u}_{\text{FEM}}||_{\max} = 0.026$ m, respectively. The error in the displacement is higher than that of the previous test cases; this is especially true for the predicted displacement at $z = 0.2$ m, where the relative error peaks at about 20%. Figs. 25 and 26 compares the displacement norm $||\boldsymbol{u}||$ of the FEM solution and of the proposed approach for $z = 0$ m and $z = 0.2$ m, respectively. Fig. 27 plots the relative equivalent plastic strain difference, normalized with respect to its maximum value $(\epsilon^{eff}_{p\,\text{FEM}})_{\max} = 0.041$, while Fig. 28 allows to appreciate the actual equivalent plastic deformation field predicted by the three dimensional FEM solution and by the proposed approach. Fig. 29 reports the cross sections stress vector $||\hat{\boldsymbol{S}} \cdot \overline{\boldsymbol{n}}||$ relative error, normalized with respect to the maximum value $||\hat{\boldsymbol{S}} \cdot \overline{\boldsymbol{n}}||_{\text{FEM max}} = 0.064$ Pa. The maximum error for the equivalent plastic strain reaches about 10%, while the normal stress vector error is kept within 2%. Fig. 30 plots the actual value of the cross section normal stress vector norm, $||\hat{\boldsymbol{S}} \cdot \overline{\boldsymbol{n}}||$, obtained with the FEM solution and the proposed approach. Both the equivalent plastic strain and the normal stress vector norm error plots show the same spatial trend, with higher plastic deformations in the middle of the cross section, suggesting that the linearization of the plastic multiplier with respect to z may be the major limiting factor for this test case. Finally, Fig. 31 plots the shear normal stress component $\hat{\boldsymbol{S}}_{yz}$, that is not constant through the cross section width.

5. Run time

The proposed procedure allows to estimate the three dimensional strain and stress fields at a given cross section as a function of the internal actions. As such, it does not give any information about what happens at different cross sections. The information provided by a three dimensional model is more comprehensive, at the expense of an increased computation time. The run times of the proposed procedure are not comparable with those of complete three dimensional solutions. Having an idea of the relative computational effort could nonetheless be of some interest. Consider the $1 \times 1 \times 10$ m clamped beam of Fig. 32, with a Green-elastic material, elastic modulus $E = 1200$ Pa and Poisson coefficient $\nu = 0.3$. A dead load per unit of reference surface $\boldsymbol{f}$ is applied in the $\boldsymbol{i}^2$ direction at the free end of the beam, $\boldsymbol{f} = 10\,\boldsymbol{i}^2$ Pa. A $10 \times 10 \times 20$ mesh with quadratic elements is first used for the three dimensional analysis. After some tuning it turns out that the fastest three dimensional solution is achieved by directly applying the whole load and using a conjugate gra-

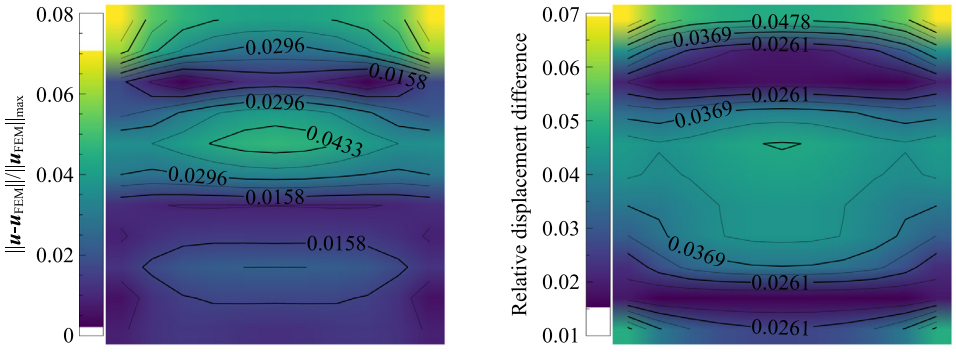

Fig. 18. Shear-bending of a Green-elastic beam: displacement relative difference, quadratic approximation, $t_y = 0.01$ N and $m_x = 0.008$ Nm; left: $z = 0$ m; right: $z = 0.2$ m.

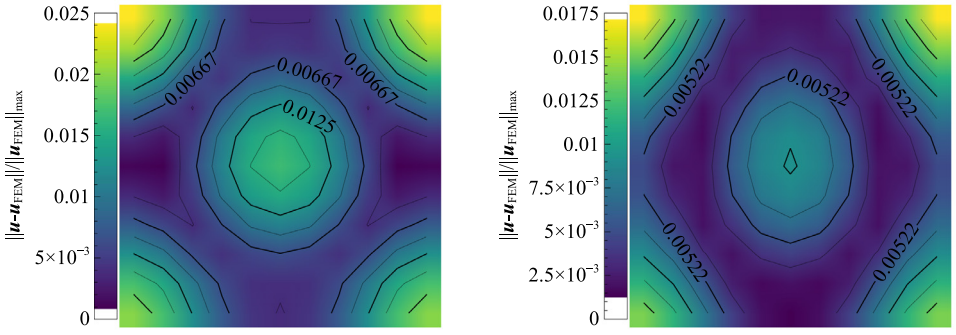

Fig. 19. Shear-bending of a Green-elastic beam: displacement relative difference, cubic approximation, $t_y = 0.01$ N and $m_x = 0.008$ Nm; left: $z = 0$ m; right: $z = 0.2$ m.

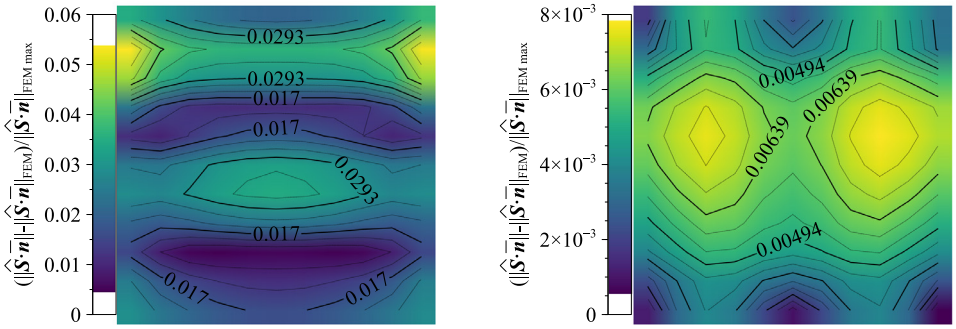

Fig. 20. Shear-bending of a Green-elastic beam: $||\hat{\boldsymbol{S}}\cdot\bar{\boldsymbol{n}}||$ relative difference, $t_y = 0.01$ N and $m_x = 0.008$ Nm; left: quadratic approximation; right: cubic approximation.

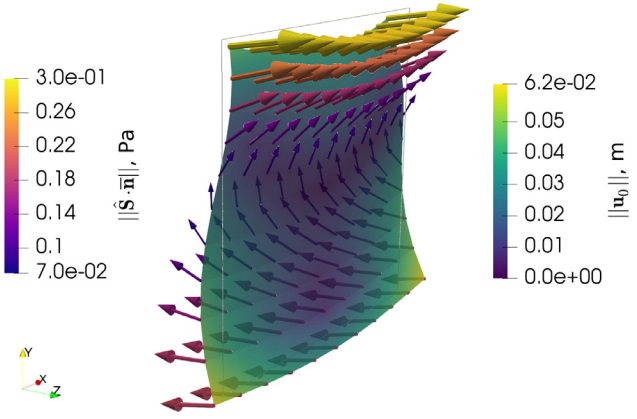

Fig. 21. Shear-bending of a Green-elastic beam: deformed configuration and normal stress vector $\hat{\boldsymbol{S}}\cdot\bar{\boldsymbol{n}}$ for $t_y = 0.05$ N and $m_x = 0.04$ Nm.

dient linear solver with an incomplete LU factorization as a preconditioner. A finer $20\times20\times40$ mesh requires at least two load steps to converge. After computing the three dimensional solutions it is possible to compute the internal actions at the clamped extremity, i.e. a shear $t_y = 10$ N together with a moment $m_x = -43.6$ Nm for the $10\times10\times20$ mesh and $m_x = -43.5$ Nm for the $20\times20\times40$ mesh; the different bending moment is due to the fact that the finer mesh, being more flexible, bends a little bit more, thus reducing the applied force arm in the deformed configuration. The computed internal loads are applied to the corresponding 10×10 and a 20×20 two-dimensional meshes built with quadratic elements and with linear, quadratic and cubic polynomial approximation in the beam axis direction. All computations were performed, with only one process, on the same hardware. Table 1 reports the time spent solving the corresponding nonlinear problems. The significantly higher run time for the finer mesh three dimensional solution allows for an increased resolution both through the cross section and along the beam axis. However, the run time ratio with respect to the two dimensional solution is not proportional to the increase resolution along the beam axis.

Table 1
Run time comparison.

	Runtime			
Cross section mesh	3D	Linear	Quadratic	Cubic
10×10	86 s	3.1 s	4.5 s	9.6 s
20×20	2504 s	4.7 s	7.2 s	25.1 s

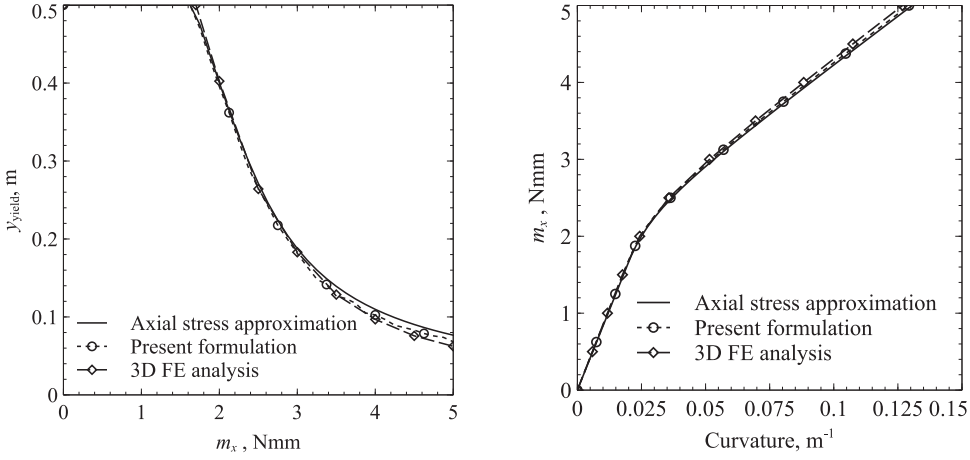

Fig. 22. Bending of an elasto-plastic beam, $m_x = 0.005$ Nm; left: elastic zone boundary y position; right: bending moment m_x as a function of the beam curvature.

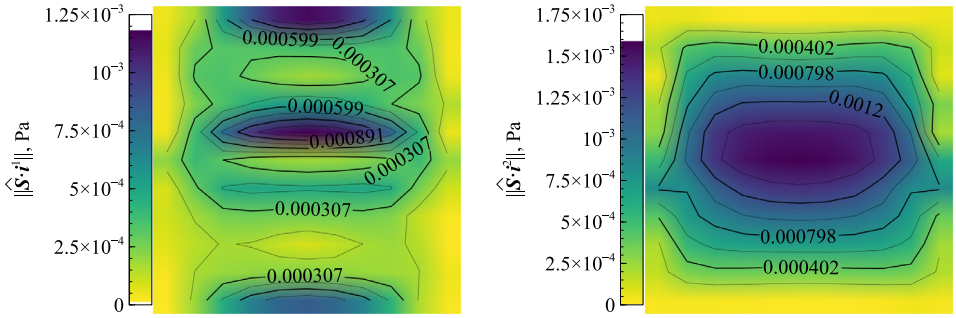

Fig. 23. Bending of an elasto-plastic beam, $m_x = 0.005$ Nm; left: $||\hat{\boldsymbol{S}}\cdot\boldsymbol{i}^1||$; right: $||\hat{\boldsymbol{S}}\cdot\boldsymbol{i}^2||$.

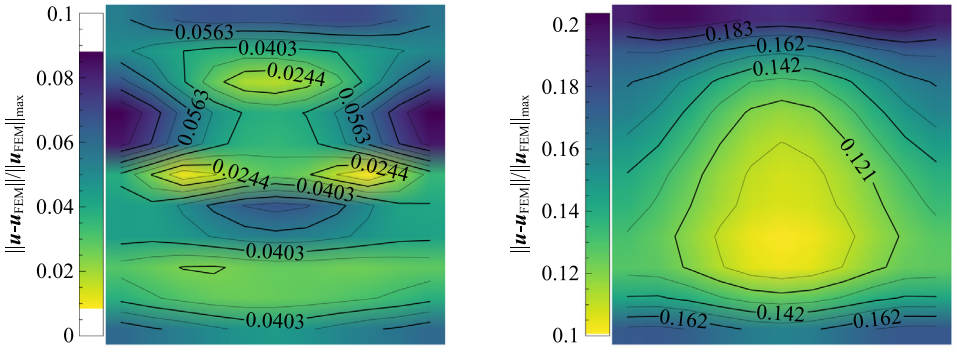

Fig. 24. Shear-bending of an elasto-plastic beam: displacement relative difference, cubic approximation, $t_y = 0.006$ N and $m_x = 0.0048$ Nm; left: $z = 0$ m; right: $z = 0.2$ m.

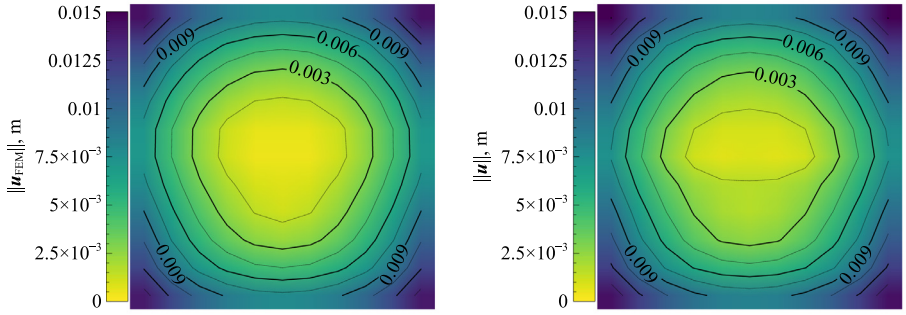

Fig. 25. Shear-bending of an elasto-plastic beam: displacement norm at $z = 0$ m; left: FEM; right: cubic approximation; $t_y = 0.006$ N and $m_x = 0.0048$ Nm.

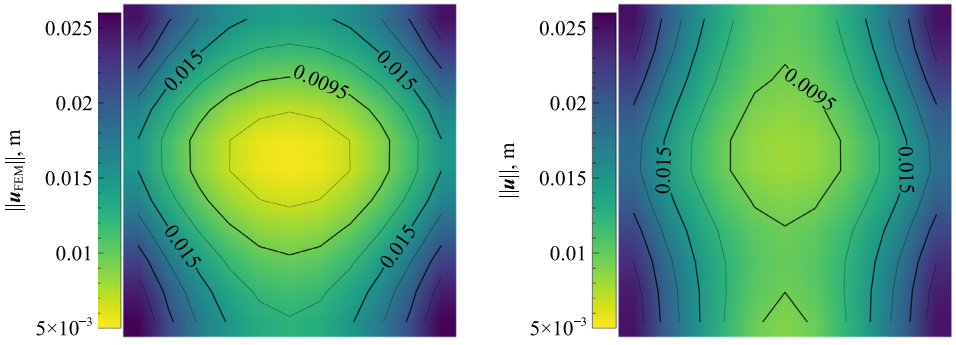

Fig. 26. Shear-bending of an elasto-plastic beam: displacement norm at $z = 0.2$ m; left: FEM; right: cubic approximation; $t_y = 0.006$ N and $m_x = 0.0048$ Nm.

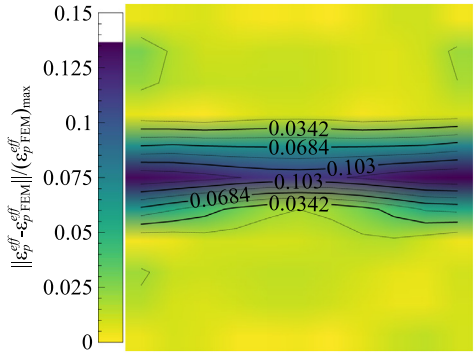

Fig. 27. Shear-bending of an elasto-plastic beam: equivalent plastic strain ϵ_p^{eff} relative difference, cubic approximation, $t_y = 0.006\,\mathrm{N}$ and $m_x = 0.0048\,\mathrm{Nm}$.

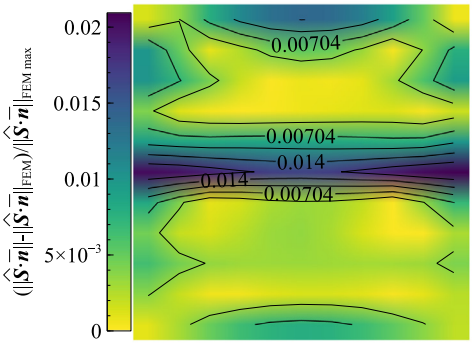

Fig. 29. Shear-bending of an elasto-plastic beam: $||\hat{\boldsymbol{S}} \cdot \overline{\boldsymbol{n}}||$ relative difference, cubic approximation, $t_y = 0.006\,\mathrm{N}$ and $m_x = 0.0048\,\mathrm{Nm}$.

6. Conclusions

A general procedure for the nonlinear approximate characterization of beam cross sections is presented. This procedure is inspired by the approach proposed by Morandini et al. (2010) and Han and Bauchau (2015a) and extends it to the nonlinear case. The degree of the polynomial approximation along the beam axis can be chosen arbitrarily.

The procedure proposed here makes no assumption whatsoever on the cross section displacement field. No attempt is made to match the deformation of the three-dimensional solid with that of a beam model. The resulting formulæare, as a consequence, really simple and almost trivial, although they hide behind them the need to derive the stress tensor with respect to the beam axis, a rather tedious task that luckily can often be delegated to a symbolic algebra engine. This simplicity has two consequences, however.

The first consequence is that the only meaningful link between the three dimensional model and the reduced beam model is given by the internal actions. One can compute the deformation of the three dimensional model that allows to achieve some given section resultants and moment resultant; it is not possible, however, to directly compute the cross section stress resultant of the three-dimensional model as a function of the beam model generalized strain. The current formulation can thus be useful to estimate the load-carrying capacity of a given cross section far from constraints and concentrated loads; it can also be used as an inverse constitutive law for formulations based on the Hellinger-Reissner principle, such as that proposed by Nukala and White (2004).

The second consequence is that the computational effort is twice that of Jiang and Yu (2015). This is because Jiang and Yu (2015) link the beam model cross section rotation and axial translation to that of the three dimensional solid, and defines the additional constant warping as a field that is superposed to this section movement in a co-rotational setting. Here, instead, no kinematic link is made, nor it is assumed a priori that the cross section do rotate and translate; thus, the minimum set of unknowns is given by the warping field and by its derivative with respect to the beam axis. If shear deformation was accounted for by Jiang and Yu (2015) two unknown fields would have likely been needed in their co-rotational setting, with the best results of the present approach obtained with four unknown fields.

It should be possible, as a future development, to account for some classes of boundary conditions and for distributed loads. Boundary conditions should be enforced by appropriate constraints applied to the first term of the expansion, $\boldsymbol{u}_0$, while distributed loads would appear at the right hand side of the nonlinear equations, see e.g. the works by Masarati (1999, Appendix E), Lin and Dong (2006) and Han and Bauchau (2015b). A different line of development could be to use the proposed approach for the multilevel nonlinear analysis of beams.

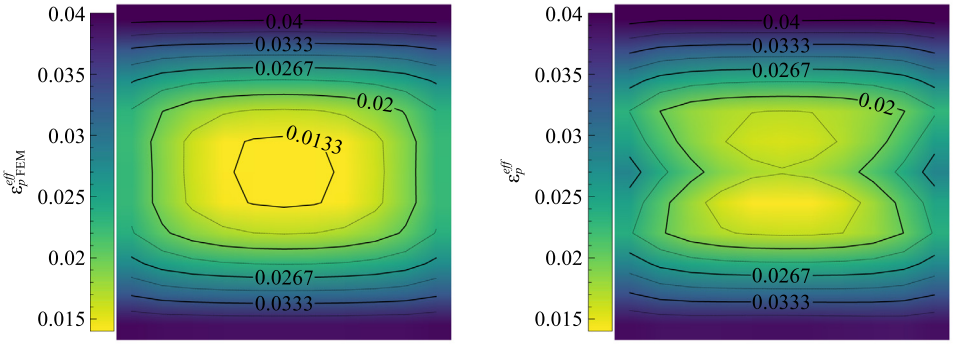

Fig. 28. Shear-bending of an elasto-plastic beam: equivalent plastic strain ϵ_p^{eff}; left: FEM; right: cubic approximation; $t_y = 0.006\,\mathrm{N}$ and $m_x = 0.0048\,\mathrm{Nm}$.

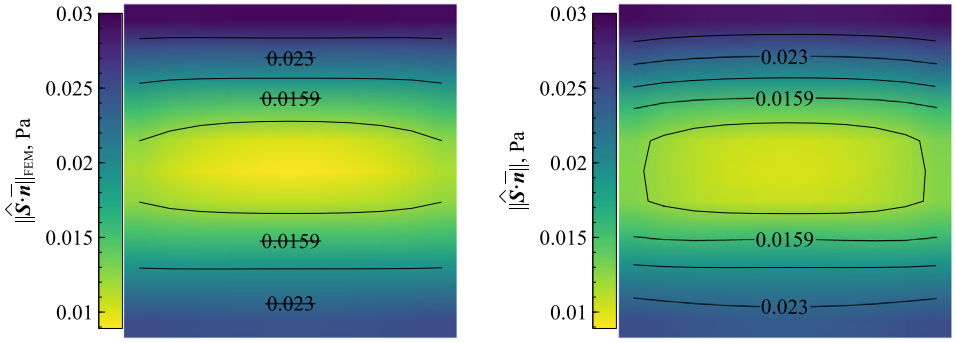

Fig. 30. Shear-bending of an elasto-plastic beam: $||\hat{\boldsymbol{S}}\cdot\bar{\boldsymbol{n}}||$; left: FEM; right: cubic approximation; $t_y = 0.006\,\mathrm{N}$ and $m_x = 0.0048\,\mathrm{Nm}$.

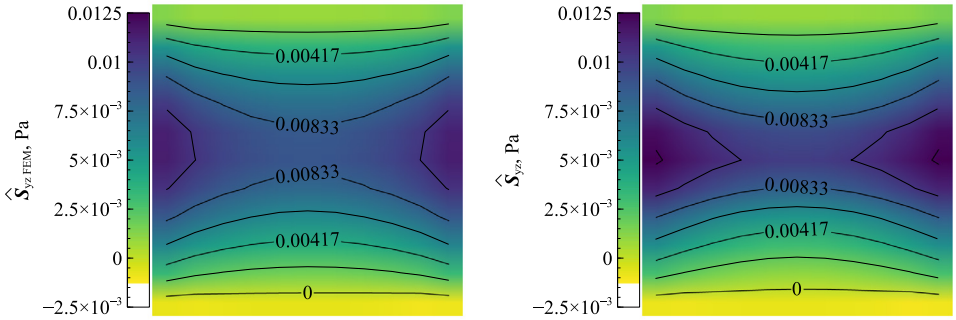

Fig. 31. Shear-bending of an elasto-plastic beam: $\hat{\boldsymbol{S}}_{yz}$; left: FEM; right: cubic approximation; $t_y = 0.006\,\mathrm{N}$ and $m_x = 0.0048\,\mathrm{Nm}$.

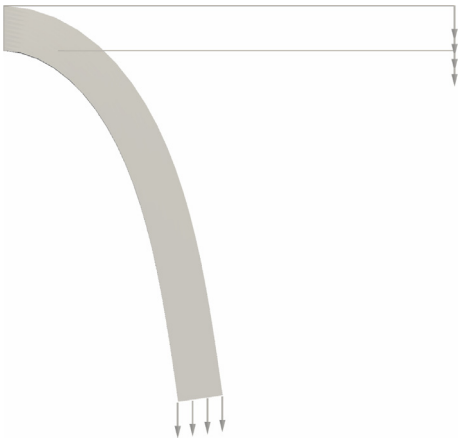

Fig. 32. Bent beam.

Appendix A. Elasto-plastic constitutive law derivatives

Consider a constitutive law with internal hidden variables $\boldsymbol{\chi}$. Since, depending on the actual constitutive law under consideration, the internal variables can have different ranks, almost all the inner product in the following are left unspecified. Let the internal energy at constant temperature be be $\psi(\boldsymbol{\epsilon}, \boldsymbol{\chi})$, so that $\boldsymbol{S} = \psi_{,\boldsymbol{\epsilon}}$ is the second Piola–Kirchhoff stress tensor and $\boldsymbol{K} = \psi_{,\boldsymbol{\chi}}$ are the thermodynamic forces. Function $f(\boldsymbol{S}, \boldsymbol{K}) \leq 0$ is the yield function; $g(\boldsymbol{S}, \boldsymbol{K})$ is a convex plastic potential, so that $-\dot{\boldsymbol{\chi}} = \dot{\lambda} g_{,\boldsymbol{K}}$. The first spatial derivative $\boldsymbol{S}_{,z}$ and $\boldsymbol{K}_{,z}$ of the stress tensor $\boldsymbol{S}$ and of the forces $\boldsymbol{K}$ with respect to z can be computed as

$$\begin{aligned}\boldsymbol{S}_{,z} &= \psi_{,\boldsymbol{\epsilon}\boldsymbol{\epsilon}} : \boldsymbol{\epsilon}_{,z} + \psi_{,\boldsymbol{\epsilon}\boldsymbol{\chi}} \boldsymbol{\chi}_{,z} \\ \boldsymbol{K}_{,z} &= \psi_{,\boldsymbol{\chi}\boldsymbol{\epsilon}} : \boldsymbol{\epsilon}_{,z} + \psi_{,\boldsymbol{\chi}\boldsymbol{\chi}} \boldsymbol{\chi}_{,z}\end{aligned} \tag{A.1}$$

where $\boldsymbol{\chi}_{,z}$ needs to be computed as function of the spatial derivative of the plastic multiplier. Assuming to have reached the yield limit $f = 0$ the spatial derivative of f is, analogously to the consistency condition,

$$f_{,\boldsymbol{S}} : \boldsymbol{S}_{,z} + f_{,\boldsymbol{K}} \boldsymbol{K}_{,z} = 0 \tag{A.2}$$

with the flow rule leading to

$$\boldsymbol{\chi}_{,z} = -g_{,\boldsymbol{K}} \lambda_{,z}. \tag{A.3}$$

Inserting Eqs. (A.1) and (A.3) into Eq. (A.2) leads to

$$f_{,\boldsymbol{S}} : \psi_{,\boldsymbol{\epsilon}\boldsymbol{\epsilon}} : \boldsymbol{\epsilon}_{,z} - f_{,\boldsymbol{S}} : \psi_{,\boldsymbol{\epsilon}\boldsymbol{\chi}} g_{,\boldsymbol{K}} \lambda_{,z} + f_{,\boldsymbol{K}} \psi_{,\boldsymbol{\chi}\boldsymbol{\epsilon}} : \boldsymbol{\epsilon}_{,z} - f_{,\boldsymbol{K}} \psi_{,\boldsymbol{\chi}\boldsymbol{\chi}} g_{,\boldsymbol{K}} \lambda_{,z} = 0$$

and, after re-arranging the terms

$$\underbrace{\left(f_{,\boldsymbol{S}} : \psi_{,\boldsymbol{\epsilon}\boldsymbol{\chi}} + f_{,\boldsymbol{K}} \psi_{,\boldsymbol{\chi}\boldsymbol{\chi}}\right) g_{,\boldsymbol{K}}}_{A} \lambda_{,z} = \underbrace{\left(f_{,\boldsymbol{S}} : \psi_{,\boldsymbol{\epsilon}\boldsymbol{\epsilon}} + f_{,\boldsymbol{K}} \psi_{,\boldsymbol{\chi}\boldsymbol{\epsilon}}\right)}_{\boldsymbol{B}} : \boldsymbol{\epsilon}_{,z} \tag{A.4}$$

the derivative of the plastic multiplier can be readily computed as

$$\lambda_{,z} = \frac{\boldsymbol{B}}{A} : \boldsymbol{\epsilon}_{,z}, \tag{A.5}$$

so that the derivative of the stress tensor becomes

$$\boldsymbol{S}_{,z} = \left(\psi_{,\boldsymbol{\epsilon}\boldsymbol{\epsilon}} - \psi_{,\boldsymbol{\epsilon}\boldsymbol{\chi}} g_{,\boldsymbol{K}} \otimes \frac{\boldsymbol{B}}{A}\right) : \boldsymbol{\epsilon}_{,z}$$

and the derivative of the forces is

$$\boldsymbol{K}_{,z} = \left(\psi_{,\boldsymbol{\chi}\boldsymbol{\epsilon}} - \psi_{,\boldsymbol{\chi}\boldsymbol{\chi}} g_{,\boldsymbol{K}} \otimes \frac{\boldsymbol{B}}{A}\right) : \boldsymbol{\epsilon}_{,z}.$$

The procedure can be repeated in order to compute the second derivative wrt. z. The first step is to derive Eq. A.1

$$\begin{aligned}\boldsymbol{S}_{,zz} &= \psi_{,\boldsymbol{\epsilon}\boldsymbol{\epsilon}\boldsymbol{\epsilon}}(\boldsymbol{\epsilon}_{,z} \otimes \boldsymbol{\epsilon}_{,z}) + 2\psi_{,\boldsymbol{\epsilon}\boldsymbol{\epsilon}\boldsymbol{\chi}}\left(\boldsymbol{\epsilon}_{,z} + \boldsymbol{\chi}_{,z}\right) + \psi_{,\boldsymbol{\epsilon}\boldsymbol{\chi}\boldsymbol{\chi}}\left(\boldsymbol{\chi}_{,z} \otimes \boldsymbol{\chi}_{,z}\right) + \psi_{,\boldsymbol{\epsilon}\boldsymbol{\epsilon}} \boldsymbol{\epsilon}_{,zz} + \psi_{,\boldsymbol{\epsilon}\boldsymbol{\chi}} \boldsymbol{\chi}_{,zz} \\ \boldsymbol{K}_{,zz} &= \psi_{,\boldsymbol{\chi}\boldsymbol{\epsilon}\boldsymbol{\epsilon}}(\boldsymbol{\epsilon}_{,z} \otimes \boldsymbol{\epsilon}_{,z}) + 2\psi_{,\boldsymbol{\chi}\boldsymbol{\epsilon}\boldsymbol{\chi}}\left(\boldsymbol{\epsilon}_{,z} + \boldsymbol{\chi}_{,z}\right) + \psi_{,\boldsymbol{\chi}\boldsymbol{\chi}\boldsymbol{\chi}}\left(\boldsymbol{\chi}_{,z} \otimes \boldsymbol{\chi}_{,z}\right) + \psi_{,\boldsymbol{\chi}\boldsymbol{\epsilon}} \boldsymbol{\epsilon}_{,zz} + \psi_{,\boldsymbol{\chi}\boldsymbol{\chi}} \boldsymbol{\chi}_{,zz}\end{aligned} \tag{A.6}$$

and the flow rule Eq. (A.3)

$$\boldsymbol{\chi}_{,zz} = -g_{,\boldsymbol{K}\boldsymbol{K}} \boldsymbol{K}_{,z} \otimes \lambda_{,z} - g_{,\boldsymbol{K}} \lambda_{,zz} - g_{,\boldsymbol{K}\boldsymbol{S}} : \boldsymbol{S}_{,z} \otimes \lambda_{,z}. \tag{A.7}$$

The second derivative of the yield function becomes

$$f_{,\boldsymbol{S}\boldsymbol{S}}(\boldsymbol{S}_{,z} \otimes \boldsymbol{S}_{,z}) + 2f_{,\boldsymbol{S}\boldsymbol{K}}(\boldsymbol{S}_{,z} \otimes \boldsymbol{K}_{,z}) + f_{,\boldsymbol{K}\boldsymbol{K}}(\boldsymbol{K}_{,z} \otimes \boldsymbol{K}_{,z}) + f_{,\boldsymbol{S}} \boldsymbol{S}_{,zz} + f_{,\boldsymbol{K}} \boldsymbol{K}_{,zz} = 0. \tag{A.8}$$

Inserting Eqs. (A.6) into Eq. (A.8)

$$\begin{aligned}&f_{,\boldsymbol{S}\boldsymbol{S}}(\boldsymbol{S}_{,z} \otimes \boldsymbol{S}_{,z}) + 2f_{,\boldsymbol{S}\boldsymbol{K}}(\boldsymbol{S}_{,z} \otimes \boldsymbol{K}_{,z}) + f_{,\boldsymbol{K}\boldsymbol{K}}(\boldsymbol{K}_{,z} \otimes \boldsymbol{K}_{,z}) \\ &\quad + f_{,\boldsymbol{S}} \psi_{,\boldsymbol{\epsilon}\boldsymbol{\epsilon}\boldsymbol{\epsilon}}(\boldsymbol{\epsilon}_{,z} \otimes \boldsymbol{\epsilon}_{,z}) + 2f_{,\boldsymbol{S}} \psi_{,\boldsymbol{\epsilon}\boldsymbol{\epsilon}\boldsymbol{\chi}}\left(\boldsymbol{\epsilon}_{,z} \otimes \boldsymbol{\chi}_{,z}\right) \\ &\quad + f_{,\boldsymbol{S}} \psi_{,\boldsymbol{\epsilon}\boldsymbol{\chi}\boldsymbol{\chi}}\left(\boldsymbol{\chi}_{,z} \otimes \boldsymbol{\chi}_{,z}\right) + f_{,\boldsymbol{S}} \psi_{,\boldsymbol{\epsilon}\boldsymbol{\epsilon}} \boldsymbol{\epsilon}_{,zz} + f_{,\boldsymbol{S}} \psi_{,\boldsymbol{\epsilon}\boldsymbol{\chi}} \boldsymbol{\chi}_{,zz} \\ &\quad + f_{,\boldsymbol{K}} \psi_{,\boldsymbol{\chi}\boldsymbol{\epsilon}\boldsymbol{\epsilon}}(\boldsymbol{\epsilon}_{,z} \otimes \boldsymbol{\epsilon}_{,z}) + 2f_{,\boldsymbol{K}} \psi_{,\boldsymbol{\chi}\boldsymbol{\epsilon}\boldsymbol{\chi}}\left(\boldsymbol{\epsilon}_{,z} \otimes \boldsymbol{\chi}_{,z}\right) + f_{,\boldsymbol{K}} \psi_{,\boldsymbol{\chi}\boldsymbol{\chi}\boldsymbol{\chi}}\left(\boldsymbol{\chi}_{,z} \otimes \boldsymbol{\chi}_{,z}\right) \\ &\quad + f_{,\boldsymbol{K}} \psi_{,\boldsymbol{\chi}\boldsymbol{\epsilon}} \boldsymbol{\epsilon}_{,zz} + f_{,\boldsymbol{K}} \psi_{,\boldsymbol{\chi}\boldsymbol{\chi}} \boldsymbol{\chi}_{,zz} = 0\end{aligned}$$

and collecting together all the terms that can be computed by knowing $\boldsymbol{\epsilon}_{,z}$ and $\lambda_{,z}$ alone,

$$\underbrace{f_{,\boldsymbol{SS}}(\boldsymbol{S}_{,z}\otimes\boldsymbol{S}_{,z})+2f_{,\boldsymbol{SK}}(\boldsymbol{S}_{,z}\otimes\boldsymbol{K}_{,z})+f_{,\boldsymbol{KK}}(\boldsymbol{K}_{,z}\otimes\boldsymbol{K}_{,z})}_{f_0}+\underbrace{\begin{bmatrix}\left(f_{,\boldsymbol{S}}\psi_{,\boldsymbol{\epsilon\epsilon\epsilon}}+f_{,\boldsymbol{K}}\psi_{,\boldsymbol{\chi\epsilon\epsilon}}\right)(\boldsymbol{\epsilon}_{,z}\otimes\boldsymbol{\epsilon}_{,z})+\\ 2\left(f_{,\boldsymbol{S}}\psi_{,\boldsymbol{\epsilon\epsilon\chi}}f_{,\boldsymbol{K}}\psi_{,\boldsymbol{\chi\epsilon\chi}}\right)\left(\boldsymbol{\epsilon}_{,z}\otimes\boldsymbol{\chi}_{,z}\right)\\ \left(f_{,\boldsymbol{S}}\psi_{,\boldsymbol{\epsilon\chi\chi}}f_{,\boldsymbol{K}}\psi_{,\boldsymbol{\chi\chi\chi}}\right)\left(\boldsymbol{\chi}_{,z}\otimes\boldsymbol{\chi}_{,z}\right)\end{bmatrix}}_{f_1}$$

$$+\underbrace{\left(f_{,\boldsymbol{S}}\psi_{,\boldsymbol{\epsilon\epsilon}}+f_{,\boldsymbol{K}}\psi_{,\boldsymbol{\chi\epsilon}}\right)}_{\boldsymbol{f}_{\boldsymbol{\epsilon}}\equiv\boldsymbol{B}}:\boldsymbol{\epsilon}_{,zz}+\underbrace{\left(f_{,\boldsymbol{S}}\psi_{,\boldsymbol{\epsilon\chi}}+f_{,\boldsymbol{K}}\psi_{,\boldsymbol{\chi\chi}}\right)}_{f_{\boldsymbol{\chi}}}\boldsymbol{\chi}_{,zz}=0$$

one gets

$$f_{\boldsymbol{\chi}}\boldsymbol{\chi}_{,zz}+\boldsymbol{B}:\boldsymbol{\epsilon}_{,zz}+f_0+f_1=0. \tag{A.9}$$

Inserting now Eq. (A.7) into Eq. (A.9) leads to

$$\underbrace{-f_{\boldsymbol{\chi}}g_{,\boldsymbol{KK}}\boldsymbol{K}_{,z}\otimes\lambda_{,z}-f_{\boldsymbol{\chi}}g_{,\boldsymbol{KS}}\boldsymbol{S}_{,z}\otimes\lambda_{,z}+f_0+f_1}_{f_2}+f_{\boldsymbol{\epsilon}}:\boldsymbol{\epsilon}_{,zz}=f_{\boldsymbol{\chi}}g_{,\boldsymbol{K}}\lambda_{,zz},$$

from which

$$\lambda_{,zz}=\frac{f_2}{f_{\boldsymbol{\chi}}g_{,\boldsymbol{K}}}+\frac{f_{\boldsymbol{\epsilon}}}{f_{\boldsymbol{\chi}}g_{,\boldsymbol{K}}}:\boldsymbol{\epsilon}_{,zz}. \tag{A.10}$$

A1. Particularization to J2 plasticity

The formulae of Appendix A become much simpler for a plasticity model based on the additive decomposition of the Green-Lagrange strain tensor into its elastic and plastic parts, $\boldsymbol{\epsilon}=\boldsymbol{\epsilon}_e+\boldsymbol{\epsilon}_p$ and with linear hardening. This model is characterized by two different internal variables, i.e. the plastic deformation and the effective plastic strain, that is equal to the plastic multiplier:

$$\boldsymbol{\chi}_1=\boldsymbol{\epsilon}_p,$$

$$\chi_2=\epsilon_p^{eff}=\lambda.$$

The yield function is given by

$$f=\sqrt{\frac{3}{2}\boldsymbol{s}:\boldsymbol{s}}-(S_0+K)=0 \tag{A.11}$$

where $\boldsymbol{s}=\boldsymbol{S}-\frac{1}{3}\boldsymbol{S}:\boldsymbol{I}$ and S_0+K is the yield equivalent stress. The forces are the opposite of the stress tensor and the increment of yield stress

$$\boldsymbol{K}_1=-\boldsymbol{S},$$

$$K_2=K.$$

The internal energy is given by

$$\psi(\boldsymbol{\epsilon},\boldsymbol{\chi})=\frac{1}{2}(\boldsymbol{\epsilon}-\boldsymbol{\epsilon}_p):\mathbb{E}:(\boldsymbol{\epsilon}-\boldsymbol{\epsilon}_p)+\frac{1}{2}H\boldsymbol{\epsilon}_p^{eff}\boldsymbol{\epsilon}_p^{eff}.$$

and an associated flow rule is assumed, i.e. $f\equiv g$.

As it is well known, this model makes sense only for small strains; with moderately large strains one should resort to the multiplicative decomposition of the deformation gradient into an elastic and plastic part, $\boldsymbol{F}=\boldsymbol{F}_e\boldsymbol{F}_p$ (see e.g. Simo and Hughes, 1998) or, at least, to a constitutive law written as a function of the logarithmic strains (Papadopoulos and Lu, 1998; 2001). Using the Green-Lagrange strain tensor and the second Piola–Kirchhoff stress tensor puts no limit to the rotation of the model; still, strains must be relatively small in order to get results matching the behavior of isotropic materials. Despite this limitation, the model has been chosen here because, with its simplicity, allows to easily check the effectiveness of the proposed formulation not only for hyperelastic constitutive laws, but also for elasto-plastic materials.

Following the notation of Appendix A the scalar A and second order tensor $\boldsymbol{B}$ of Eq. (A.4) become

$$\begin{aligned}A&=\left(f_{,\boldsymbol{S}}:\psi_{,\boldsymbol{\epsilon\chi}}+f_{,\boldsymbol{K}}\psi_{,\boldsymbol{\chi\chi}}\right)g_{,\boldsymbol{K}}\\&=f_{,\boldsymbol{S}}:\mathbb{E}:f_{,\boldsymbol{S}}+H\\&=f_{,\boldsymbol{S}}:\mathbb{E}:f_{,\boldsymbol{S}}+H,\end{aligned}$$

$$\begin{aligned}\boldsymbol{B}&=f_{,\boldsymbol{S}}:\psi_{,\boldsymbol{\epsilon\epsilon}}+f_{,\boldsymbol{K}}\psi_{,\boldsymbol{\chi\epsilon}}\\&=f_{,\boldsymbol{S}}:\mathbb{E}\end{aligned}$$

The derivative of the stress tensor is equal to

$$\boldsymbol{S}_{,z} = \underbrace{\left(\mathbb{E} - \mathbb{E} : f_{,\boldsymbol{S}} \otimes \frac{\boldsymbol{B}}{A}\right)}_{\mathbb{E}_{,z}} : \boldsymbol{\epsilon}_{,z}$$

$$= \mathbb{E}_{,z} : \boldsymbol{\epsilon}_{,z}. \tag{A.12}$$

Computing now the coefficients of Eq. (A.9) one gets

$$f_0 = f_{,\boldsymbol{SS}}(\boldsymbol{S}_{,z} \otimes \boldsymbol{S}_{,z})$$

and

$$f_1 = 0$$

because all the third derivatives of ψ are null. Then, since

$$\boldsymbol{f}_{\boldsymbol{\epsilon}} \equiv \boldsymbol{B}$$
$$= f_{,\boldsymbol{S}} : \mathbb{E}$$

and

$$f_{\boldsymbol{\chi}} \boldsymbol{\chi}_{,zz} = -f_{,\boldsymbol{S}} : \mathbb{E} : \boldsymbol{\epsilon}_{p,zz} - H\lambda_{,zz}$$

Eq. (A.9) becomes

$$\begin{pmatrix} f_{,\boldsymbol{S}} : \mathbb{E} : f_{,\boldsymbol{SS}} : -\boldsymbol{S}_{,z}\lambda_{,z} \\ +f_1 + f_0 \end{pmatrix} + f_{,\boldsymbol{S}} : \mathbb{E} : \boldsymbol{\epsilon}_{,zz}$$
$$= -f_{,\boldsymbol{S}} : \mathbb{E} : f_{,\boldsymbol{SS}} : \boldsymbol{S}_{,z}\lambda_{,z} + \underbrace{f_{,\boldsymbol{SS}}(\boldsymbol{S}_{,z} \otimes \boldsymbol{S}_{,z})}_{f_0} + f_{,\boldsymbol{S}} : \mathbb{E} : \boldsymbol{\epsilon}_{,zz}$$
$$= (f_{,\boldsymbol{S}} : \mathbb{E} : f_{,\boldsymbol{S}} + H)\lambda_{,zz}$$

so that the second derivative $\lambda_{,zz}$ of the plastic multiplier is

$$\lambda_{,zz} = \frac{-f_{,\boldsymbol{S}} : \mathbb{E} : f_{,\boldsymbol{SS}} : \boldsymbol{S}_{,z} \otimes \lambda_{,z} + \underbrace{f_{,\boldsymbol{SS}}(\boldsymbol{S}_{,z} \otimes \boldsymbol{S}_{,z})}_{f_0} + f_{,\boldsymbol{S}} : \mathbb{E} : \boldsymbol{\epsilon}_{,zz}}{(f_{,\boldsymbol{S}} : \mathbb{E} : f_{,\boldsymbol{S}} + H)}$$
$$= \frac{-f_{,\boldsymbol{S}} : \mathbb{E} : f_{,\boldsymbol{SS}} : \mathbb{E}_{,z} : \boldsymbol{\epsilon}_{,z} \otimes \frac{\boldsymbol{B}}{A} : \boldsymbol{\epsilon}_{,z} + f_{,\boldsymbol{SS}} \vdots (\mathbb{E}_{,z} : \boldsymbol{\epsilon}_{,z} \otimes \mathbb{E}_{,z} : \boldsymbol{\epsilon}_{,z}) + f_{,\boldsymbol{S}} : \mathbb{E} : \boldsymbol{\epsilon}_{,zz}}{(f_{,\boldsymbol{S}} : \mathbb{E} : f_{,\boldsymbol{S}} + H)}$$

and

$$\boldsymbol{\epsilon}_{p,zz} = f_{,\boldsymbol{SS}} : \boldsymbol{S}_{,z} \otimes \lambda_{,z} + f_{,\boldsymbol{S}}\lambda_{,zz} = f_{,\boldsymbol{SS}} : \mathbb{E}_{,z} : \boldsymbol{\epsilon}_{,z} \otimes \frac{\boldsymbol{B}}{A} : \boldsymbol{\epsilon}_{,z}$$
$$+ f_{,\boldsymbol{S}} \frac{1}{(f_{,\boldsymbol{S}} : \mathbb{E} : f_{,\boldsymbol{S}} + H)} \begin{bmatrix} \left(-f_{,\boldsymbol{S}} : \mathbb{E} : f_{,\boldsymbol{SS}} : \mathbb{E}_{,z} \otimes \frac{\boldsymbol{B}}{A}\right) \vdots (\boldsymbol{\epsilon}_{,z} \otimes \boldsymbol{\epsilon}_{,z}) \\ + f_{,\boldsymbol{SS}} \vdots (\mathbb{E}_{,z} : \boldsymbol{\epsilon}_{,z} \otimes \mathbb{E}_{,z} : \boldsymbol{\epsilon}_{,z}) + f_{,\boldsymbol{S}} : \mathbb{E} : \boldsymbol{\epsilon}_{,zz} \end{bmatrix}$$
$$= \tilde{\mathbb{A}} \vdots (\boldsymbol{\epsilon}_{,z} \otimes \boldsymbol{\epsilon}_{,z}) + f_{,\boldsymbol{S}}\tilde{\boldsymbol{B}} : \boldsymbol{\epsilon}_{,zz},$$

where tensor $\tilde{\mathbb{A}}$ collects all the terms that multiply $(\boldsymbol{\epsilon}_{,z} \otimes \boldsymbol{\epsilon}_{,z})$ and $\tilde{\boldsymbol{B}} = (f_{,\boldsymbol{S}} : \mathbb{E})/A$. Since both $\mathbb{E}$ and $\mathbb{E}_{,z} = (\mathbb{E} - \mathbb{E} : f_{,\boldsymbol{S}} \otimes f_{,\boldsymbol{S}} : \mathbb{E} * \frac{1}{A})$ have major symmetry, $\boldsymbol{B} = f_{,\boldsymbol{S}} : \mathbb{E} = \boldsymbol{B}^T$, $A = f_{,\boldsymbol{S}} : \mathbb{E} : f_{,\boldsymbol{S}} + H$ and $\boldsymbol{C} = f_{,\boldsymbol{S}} : \mathbb{E} = \boldsymbol{C}^T$. The fourth order tensor $\tilde{\mathbb{A}}$ can thus be rewritten as

$$\tilde{\mathbb{A}} = f_{,\boldsymbol{SS}} : \mathbb{E}_{,z} \otimes \frac{\boldsymbol{B}}{A} + \frac{f_{,\boldsymbol{S}}}{A}\left[\left(-f_{,\boldsymbol{S}} : \mathbb{E} : f_{,\boldsymbol{SS}} : \mathbb{E}_{,z} \otimes \frac{\boldsymbol{B}}{A}\right) + \mathbb{E}_{,z} : f_{,\boldsymbol{SS}} : \mathbb{E}_{,z}\right]$$

so that

$$\begin{aligned} \boldsymbol{S}_{,zz} &= \psi_{,\boldsymbol{\epsilon\epsilon\epsilon}}(\boldsymbol{\epsilon}_{,z} \otimes \boldsymbol{\epsilon}_{,z}) + 2\psi_{,\boldsymbol{\epsilon\epsilon\chi}}\left(\boldsymbol{\epsilon}_{,z} + \boldsymbol{\chi}_{,z}\right) + \psi_{,\boldsymbol{\epsilon\chi\chi}}\left(\boldsymbol{\chi}_{,z} \otimes \boldsymbol{\chi}_{,z}\right) + \psi_{,\boldsymbol{\epsilon\epsilon}}\boldsymbol{\epsilon}_{,zz} + \psi_{,\boldsymbol{\epsilon\chi}}\boldsymbol{\chi}_{,zz} \\ &= \mathbb{E} : (\boldsymbol{\epsilon}_{,zz} - \boldsymbol{\epsilon}_{p,zz}) \\ &= \left(\mathbb{E} - \mathbb{E} : f_{,\boldsymbol{S}} \otimes \tilde{\boldsymbol{B}}\right) : \boldsymbol{\epsilon}_{,zz} - \mathbb{E} : \tilde{\mathbb{A}} \vdots (\boldsymbol{\epsilon}_{,z} \otimes \boldsymbol{\epsilon}_{,z}). \end{aligned} \tag{A.13}$$

Eqs. (A.12) and (A.13) make clear that, while the first derivative $\boldsymbol{S}_{,z}$ of the stress tensor depends only on the first derivative of the strain tensor, the second derivative $\boldsymbol{S}_{,zz}$ is a function of both $\boldsymbol{\epsilon}_{,z}$ and $\boldsymbol{\epsilon}_{,zz}$.

Appendix B. Three-dimensional solid loads

As explained in Section 4 the validation is performed by comparing the results obtained with the proposed approach with those obtained with a three dimensional model that is loaded at its two extremities in such a way that the middle section at $z = 0$ m reacts with the sought internal actions $\boldsymbol{t}$ and $\boldsymbol{m}$. To this end, distributed loads are applied at its two extremity section A_1 and A_2, with a constant

contribution ($\boldsymbol{\lambda}_{F_1}$ on A_1 and $\boldsymbol{\lambda}_{F_2}$ on A_2) added to two follower linearly varying normal contributions (proportional to $\lambda_{M_1 1}$ and $\lambda_{M_1 2}$ on A_1, $\lambda_{M_2 1}$ and $\lambda_{M_2 2}$ on A_2) and to a follower torsion-like contribution (proportional to $\lambda_{M_1 3}$ on A_1 and $\lambda_{M_2 3}$ on A_2):

$$\boldsymbol{t}_{A_1} = \boldsymbol{\lambda}_{F_1} + \left(\frac{\boldsymbol{F}^{-T}\boldsymbol{i}^2}{\left\| \boldsymbol{F}^{-T}\boldsymbol{i}^2 \right\|} x_1 - \frac{\boldsymbol{F}^{-T}\boldsymbol{i}^1}{\left\| \boldsymbol{F}^{-T}\boldsymbol{i}^1 \right\|} x_2 \right) \lambda_{M_1 3} + \frac{\boldsymbol{F}^{-T}\boldsymbol{i}^3}{\left\| \boldsymbol{F}^{-T}\boldsymbol{i}^3 \right\|} (x_2 \lambda_{M_1 1} + x_1 \lambda_{M_1 2}),$$

$$\boldsymbol{t}_{A_2} = \boldsymbol{\lambda}_{F_2} + \left(\frac{\boldsymbol{F}^{-T}\boldsymbol{i}^2}{\left\| \boldsymbol{F}^{-T}\boldsymbol{i}^2 \right\|} x_1 - \frac{\boldsymbol{F}^{-T}\boldsymbol{i}^1}{\left\| \boldsymbol{F}^{-T}\boldsymbol{i}^1 \right\|} x_2 \right) \lambda_{M_2 3} + \frac{\boldsymbol{F}^{-T}\boldsymbol{i}^3}{\left\| \boldsymbol{F}^{-T}\boldsymbol{i}^3 \right\|} (x_2 \lambda_{M_2 1} + x_1 \lambda_{M_2 2}).$$

The values of vectors $\boldsymbol{\lambda}_{F_{(1,2)}}$ and $\boldsymbol{\lambda}_{M_{(1,2)}}$ are computed by imposing twelve equations. The first six equations states that the resultant of the loads on one of the two faces must be equal to sought value of the stress resultant $\boldsymbol{t}$ and that the moment resultant of the same loads, computed with respect to the origin, must be equal to the sough moment resultant $\boldsymbol{m}$:

$$\int_{A_1} \boldsymbol{t}_{A_1} \mathrm{d}A = \boldsymbol{t},$$

$$\int_{A_1} \boldsymbol{x} \times \boldsymbol{t}_{A_1} \mathrm{d}A = \boldsymbol{m}.$$

The missing six equations impose that the overall resultant and moment resultant of the external loads must be null:

$$\int_{A_1} \boldsymbol{t}_{A_1} \mathrm{d}A + \int_{A_2} \boldsymbol{t}_{A_2} \mathrm{d}A = \boldsymbol{0},$$

$$\int_{A_1} \boldsymbol{x} \times \boldsymbol{t}_{A_1} \mathrm{d}A + \int_{A_2} \boldsymbol{x} \times \boldsymbol{t}_{A_2} \mathrm{d}A = \boldsymbol{0}.$$

Appendix C. Implementation

A reference implementation for the Neo-Hookean hyperelastic material is reported below. Note that dealing with elasto-plastic materials is significantly harder in Dolfin, since one has to explicitly deal with the stress evaluated at different integration points and to write his own code for the return mapping; to this end, the fenics-solid-mechanics library, currently available from https://bitbucket.org/fenics-apps/fenics-solid-mechanics/src/master/, was modified and extended with the formulæ of Appendix A.1. More in detail (see e.g. Logg and Wells (2010); Logg et al. (2012b); Alnæs et al. (2014) for an introduction to the Unified Form Laguage UFL, the Fenics Form Compiler FFC and, more generally, to Dolfin), Dolfin provides an abstraction for fields that can be evaluated only at integration points, the so-called `Quadrature` elements. Three additional classes are built starting from this abstraction, in such a way that their instances can be used within an UFL form and understood by the FFC form compiler. The first one, called `UFLQuadratureFunction`, allows to evaluate the values of an arbitrary UFL expression at the integration points of any given element; this is used for computing the Green-Lagrange strain tensor $\boldsymbol{\epsilon}$ and its derivatives wrt. z at the integration points. The second one, called `QuadratureFunction`, is used to return the stress tensor, its derivatives wrt. z and all the required tangent moduli, as computed by the return mapping procedure. The third one, `HistoryData`, is used to store the values of hidden variables, such as the plastic strain $\boldsymbol{\epsilon}_p$, both for the current and the last converged load step. Whenever the form assembly requires, for a given element, the value of any of these `QuadratureFunction` class instances, a standard hand-coded return mapping procedure is called, the current values of the `HistoryData` variables are updated, and the computed values are returned to the calling procedure. Caching of results allows to avoid repetitive calls, at the element level, of the return mapping procedure.

```
# Copyright 2018 Marco Morandini
#
# This program is free software: you can redistribute it and/or modify
# it under the terms of the GNU General Public License as published by
# the Free Software Foundation, either version 3 of the License, or
# (at your option) any later version.
#
# This program is distributed in the hope that it will be useful,
# but WITHOUT ANY WARRANTY; without even the implied warranty of
# MERCHANTABILITY or FITNESS FOR A PARTICULAR PURPOSE.
# See the GNU General Public License for more details.
#
# You should have received a copy of the GNU General Public License
# along with this program.
# If not, see <https://www.gnu.org/licenses/>.

from dolfin import *
# cubic elements in plane
element_order = 3
parameters["form_compiler"]["quadrature_degree"] = 4
FOR_IA = Constant((0., 0., 0.))
MOM_IA = Constant((0., 0., 0.))
E = Constant(1.)
nu = Constant(0.33)
mu = E / (2.0*(1.0 + nu))
lmbda = E*nu / ((1.0 + nu)*(1.0 - 2.0*nu))
def grad3d(u, up):
    "Return 3d gradient."
    g = grad(u)
    return as_tensor([[g[0,0],g[0,1],up[0]],[g[1,0],g[1,1], \
        up[1]],[g[2,0],g[2,1],up[2]]])
def DefGradient(u, up):
    "Return 3d deformation gradient."
    g = grad(u)
    return as_tensor([[g[0,0]+1.,g[0,1],up[0]], \
        [g[1,0],g[1,1]+1.,up[1]],[g[2,0],g[2,1],up[2]+1.]])
```

```
def epsilon(defgrad):
    "Return symmetric 3D deformation tensor."
    return 0.5*(dot(defgrad.T, defgrad)-Identity(3))
def pos3d(POS):
    return as_vector([POS[0], POS[1], 0.])
def AbaqusNeoHookean1pkStress(defgrad):
    "Return NeoHookean (Abaqus version) 1 PK stress tensor."
    C10 = mu / 2.
    K0 = E / (3. * (1. - 2. * nu))
    F = defgrad
    F = variable(F)
    J = det(F)
    Fdev = pow(J, -1./3.) * F
    I1 = pow(J, -2./3.) * tr(F.T*F)
    psi = C10 * (I1 - 3.) + (J - 1.) * (J - 1.) * K0 / 2.
    first_PK = diff(psi, F)
    return first_PK
#10x10 mesh centered in (0, 0)
mesh = UnitSquareMesh(10, 10)
ALE.move(mesh, Constant([-0.5, -0.5]))
# axial coordinate
Z_ELEMENT = FiniteElement("R", mesh.ufl_cell(), 0)
Z_SPACE = FunctionSpace(mesh, Z_ELEMENT)
Z = Function(Z_SPACE)
Z.interpolate(Constant(0.))
UF3_ELEMENT = VectorElement("CG", mesh.ufl_cell(), element_order, 3)
# Lagrange multipliers needed to compute
# the stress resultants and moment resultants
R3_ELEMENT = VectorElement("R", mesh.ufl_cell(), 0, 3)
RLAGR_ELEMENT = VectorElement("R", mesh.ufl_cell(), 0, 6)
FU36_ELEMENT = MixedElement(UF3_ELEMENT, UF3_ELEMENT, \
    R3_ELEMENT, R3_ELEMENT, \
    RLAGR_ELEMENT, UF3_ELEMENT, UF3_ELEMENT)
FU36_SPACE = FunctionSpace(mesh, FU36_ELEMENT)
FU36 = Function(FU36_SPACE, name="u")
FU36_s = split(FU36)
VU36 = TestFunction(FU36_SPACE)
```

```
TU36 = TrialFunction(FU36_SPACE)
VU36_s = split(VU36)
# deformed position = undeformed position + displacement
POS = MeshCoordinates(mesh)
POSp = pos3d(POS) + FU36_s[0]
# vector fields need to compute stress resultants
# and impose constraints
Torsion = as_tensor([-POS[1], POS[0], 0.])
Flex_y = as_tensor([0., 0., -POS[0]])
Flex_x = as_tensor([0., 0., POS[1]])
X_translation = as_tensor([1., 0., 0.])
Y_translation = as_tensor([0., 1., 0.])
Z_translation = as_tensor([0., 0., 1.])
# displacement approximation
U = FU36_s[0]
U += FU36_s[1] * Z
U += 0.5 * FU36_s[5] * Z * Z
U += 1./6. * FU36_s[6] * Z * Z * Z
# first and second derivative of displacement wrt Z
dUdz = diff(U, Z)
dUdz2 = diff(dUdz, Z)
# deformation gradient
F = DefGradient(U, dUdz)
dFdz = diff(F, Z)
dFdz2 = diff(dFdz, Z)
delta_F = derivative(F, FU36, VU36)
delta_Fn = delta_F[:,2]
delta_F1 = delta_F[:,0]
delta_F2 = delta_F[:,1]
delta_Fs = as_tensor([[delta_F1[0], delta_F2[0]], \
    [delta_F1[1], delta_F2[1]], \
    [delta_F1[2], delta_F2[2]]])
delta_Fndz = diff(delta_Fn, Z)
delta_Fndz2 = diff(delta_Fndz, Z)
ddelta_Fsdz = diff(delta_Fs, Z)
ddelta_Fsdz2 = diff(ddelta_Fsdz, Z)
```

```
ddelta_Fsdz3 = diff(ddelta_Fsdz2, Z)
# 1 PK stress tensor and its derivatieves
S = AbaqusNeoHookean1pkStress(F)
Sn = S[:,2]
S1 = S[:,0]
S2 = S[:,1]
Ss = as_tensor([[S1[0], S2[0]], [S1[1], S2[1]], [S1[2], S2[2]]])
dSndz = diff(Sn, Z)
dSndz2 = diff(dSndz, Z)
dSndz3 = diff(dSndz2, Z)
dSndz4 = diff(dSndz3, Z)
dSsdz = diff(Ss, Z)
dSsdz2 = diff(dSsdz, Z)
dSsdz3 = diff(dSsdz2, Z)
# equilibrium equations
Eq = - dot(VU36_s[0], dSndz) * dx + inner(delta_Fs, Ss) * dx
Eq -= dot(VU36_s[1], dSndz) * dx + inner(ddelta_Fsdz, Ss) * dx
Eq -= dot(VU36_s[0], dSndz2) * dx + inner(delta_Fs, dSsdz) * dx
Eq -= dot(VU36_s[5], dSndz) * dx + inner(ddelta_Fsdz2, Ss) * dx
Eq -= dot(VU36_s[1], dSndz2) * dx + inner(ddelta_Fsdz, dSsdz) * dx
Eq -= dot(VU36_s[1], dSndz2) * dx + inner(ddelta_Fsdz, dSsdz) * dx
Eq -= dot(VU36_s[0], dSndz3) * dx + inner(delta_Fs, dSsdz2) * dx
Eq -= dot(VU36_s[6], dSndz) * dx + inner(ddelta_Fsdz3, Ss) * dx
Eq -= dot(VU36_s[5], dSndz2) * dx + inner(ddelta_Fsdz2, dSsdz) * dx
Eq -= dot(VU36_s[5], dSndz2) * dx + inner(ddelta_Fsdz2, dSsdz) * dx
Eq -= dot(VU36_s[1], dSndz3) * dx + inner(ddelta_Fsdz, dSsdz2) * dx
Eq -= dot(VU36_s[5], dSndz2) * dx + inner(ddelta_Fsdz2, dSsdz) * dx
Eq -= dot(VU36_s[1], dSndz3) * dx + inner(ddelta_Fsdz, dSsdz2) * dx
Eq -= dot(VU36_s[1], dSndz3) * dx + inner(ddelta_Fsdz, dSsdz2) * dx
Eq -= dot(VU36_s[0], dSndz4) * dx + inner(delta_Fs, dSsdz3) * dx
# equivalence of internal actions
Force = dot(VU36_s[2], Sn) * dx - dot(VU36_s[2], FOR_IA) * dx
Force += dot(FU36_s[2], derivative(Sn, FU36, VU36)) * dx
Moment = dot(VU36_s[3], cross(POSp, Sn)) * dx
Moment -= dot(VU36_s[3], MOM_IA) * dx
Moment += dot(FU36_s[3], derivative(cross(POSp, Sn), FU36, VU36)) * dx
LinearForm = Eq + Force + Moment
```

```
# constraints on average rigid body motions
LinearForm += VU36_s[4][0] * FU36_s[0][0] * dx
LinearForm += FU36_s[4][0] * VU36_s[0][0] * dx
LinearForm += VU36_s[4][1] * FU36_s[0][1] * dx
LinearForm += FU36_s[4][1] * VU36_s[0][1] * dx
LinearForm += VU36_s[4][2] * FU36_s[0][2] * dx
LinearForm += FU36_s[4][2] * VU36_s[0][2] * dx
LinearForm += VU36_s[4][3] * dot(FU36_s[0], Torsion) * dx
LinearForm += FU36_s[4][3] * dot(VU36_s[0], Torsion) * dx
LinearForm += VU36_s[4][4] * dot(FU36_s[0], Flex_x) * dx
LinearForm += FU36_s[4][4] * dot(VU36_s[0], Flex_x) * dx
LinearForm += VU36_s[4][5] * dot(FU36_s[0], Flex_y) * dx
LinearForm += FU36_s[4][5] * dot(VU36_s[0], Flex_y) * dx
# number of increments and target internal actions
num_incs = 20
FIN_Tx = 0.
FIN_Ty = 0.05
FIN_N = 0.
FIN_Mx = 0.04
FIN_My = 0.0
FIN_Mz = 0.
# loop over load steps
for i in range(1, num_incs + 1, 1):
    # assign the actual value of sought internal action
    # for this load step
    FOR_IA.assign(Constant((FIN_Tx / num_incs * i, \
        FIN_Ty / num_incs * i, FIN_N / num_incs * i )))
    MOM_IA.assign(Constant((FIN_Mx / num_incs * i, \
        FIN_My / num_incs * i, FIN_Mz / num_incs * i )))
    # actually solve the nonlinear problem
    solve(LinearForm==0, FU36)
```

References

Alnæs, M.S., Blechta, J., Hake, J., Johansson, A., Kehlet, B., Logg, A., Richardson, C., Ring, J., Rognes, M.E., Wells, G.N., 2015. The fenics project version 1.5. Arch. Numer. Softw. 3 (100). doi:10.11588/ans.2015.100.20553.

Alnæs, M.S., Logg, A., Ølgaard, K.B., Rognes, M.E., Wells, G.N., 2014. Unified form language: a domain-specific language for weak formulations of partial differential equations. ACM Trans. Math. Softw. 40 (2). doi:10.1145/2566630.

Berdichevsky, V.L., 1981. On the energy of an elastic rod. J. Appl. Math. Mech. 45 (4), 518–529. doi:10.1016/0021-8928(81)90097-6.

Borri, M., Ghiringhelli, G.L., Merlini, T., 1992. Linear analysis of naturally curved and twisted anisotropic beams. Compos. Eng. 2 (5–7), 433–456. doi:10.1016/0961-9526(92)90036-6.

Borri, M., Merlini, T., 1986. A large displacement formulation for anisotropic beam analysis. Meccanica 21 (1), 30–37. doi:10.1007/BF01556314.

Cardona, A., Geradin, M., 1988. A beam finite element non-linear theory with finite rotations. Int. J. Numer. Methods Eng. 26, 2403–2438.

Cesnik, C.E.S., 1994. Cross-sectional analysis of initially twisted and curved composite beams. Ph.D. thesis. Georgia Institute of Technology.

Chakravarty, U.K., 2011. On the modeling of composite beam cross-sections. Compos. Part B 42 (4), 982–991. doi:10.1016/j.compositesb.2010.10.012.

Chiorean, C.G., 2017. Second-order flexibility-based model for nonlinear inelastic analysis of 3d semi-rigid steel frameworks. Eng. Struct. 136, 547–579. doi:10.1016/j.engstruct.2017.01.040.

Corre, G., Lebée, A., Sab, K., Ferradi, M.K., Cespedes, X., 2018. The asymptotic expansion load decomposition elastoplastic beam model. Int. J. Numer. Methods Eng. 116 (5), 308–331. doi:10.1002/nme.5926.

Druz, A.N., Polyakov, N.A., Ustinov, Y.A., 1996. Homogeneous solutions and Saint–Venant problems for a naturally twisted rod. J. Appl. Math. Mech. 60 (4), 657–664.

Ferradi, M.K., Lebée, A., Fliscounakis, A., Cespedes, X., Sab, K., 2016. A model reduction technique for beam analysis with the asymptotic expansion method. Comput. Struct. 172, 11–28. doi:10.1016/j.compstruc.2016.05.013.

Garcea, G., Gonçalves, R., Bilotta, A., Manta, D., Bebiano, R., Leonetti, L., Magisano, D., Camotim, D., 2016. Deformation modes of thin-walled members: a comparison between the method of generalized eigenvectors and generalized beam theory. Thin-Walled Struct. 100, 192–212. doi:10.1016/j.tws.2015.11.013.

Giavotto, V., Borri, M., Mantegazza, P., Ghiringhelli, G.L., Carmaschi, V., Maffioli, G.C., Mussi, F., 1983. Anisotropic beam theory and applications. Comput. Struct. 16, 403–413.

Han, S., Bauchau, O.A., 2014. Nonlinear three-dimensional beam theory for flexible multibody dynamics. Multibody Syst. Dyn. 1–32. doi:10.1007/s11044-014-9433-8.

Han, S., Bauchau, O.A., 2015a. On Saint–Venant's problem for helicoidal beams. J. Appl. Mech. 83 (2). 021009–021009. doi: 10.1115/1.4031935.

Han, S., Bauchau, O.A., 2015b. On the solution of Almansi–Michell's problem. Int. J. Solids Struct. 75–76, 156–171. doi:10.1016/j.ijsolstr.2015.08.010.

Han, S., Bauchau, O.A., 2016. On the analysis of periodically heterogenous beams. J. Appl. Mech. 83 (9). 091001–1–091001–13. doi: 10.1115/1.4033721.

Hodges, D.H., 2006. Nonlinear Composite Beam Theory. No. 213. Progress in Astronautics and Aeronautics. American Institute of Aeronautics and Astronautics, 1801 Alexander Bell Drive, Suite 500, Reston, VA, 20191-4344, USA.

Ieşan, D., 1976. Saint–Venant's problem for inhomogeneous and anisotropic elastic bodies. J. Elast. 6 (3), 277–294. doi:10.1007/BF00041722.

Ieşan, D., 2008. Classical and Generalized Models of Elastic Rods. CRC Press. Google–Books-ID: 7KBJ34lHTsUC

Jiang, F., Deo, A., Yu, W., 2018. A composite beam theory for modeling nonlinear shear behavior. Eng. Struct. 155, 73–90. doi:10.1016/j.engstruct.2017.10.051.

Jiang, F., Yu, W., 2015. Nonlinear variational asymptotic sectional analysis of hyperelastic beams. AIAA J. doi:10.2514/1.J054334.

Lin, H.-C., Dong, S.B., 2006. On the Almansi–Michell problems for an inhomogeneous, anisotropic cylinder. J. Mech. 22 (1), 51–57. doi:10.1017/S1727719100000782.

Logg, A., Mardal, K.-A., Wells, G.N., et al., 2012a. Automated Solution of Differential Equations by the Finite Element Method. Springer doi:10.1007/978-3-642-23099-8.

Logg, A., Wells, G.N., 2010. Dolfin: automated finite element computing. ACM Trans. Math. Softw. 37 (2). doi:10.1145/1731022.1731030.

Logg, A., Wells, G.N., Hake, J., 2012b. DOLFIN: a C++/Python Finite Element Library. Springer. Ch. 10

Masarati, P., 1999. Comprehensive multibody aeroservoelastic analysis of integrated rotorcraft active controls: dottorato di ricerca in ingegneria aerospaziale / Pierangelo Masarati ; tutor: Paolo Mantegazza ; \Politecnico di Milano! Ph.D. Thesis. Politecnico di Milano, Milano. URL https://home.aero.polimi.it/masarati/Publications/thesis.pdf

Merlini, T., 1988. On the development of static modes in slender elements under end loads. Aerotecnica – missili e spazio 67 (1–4), 104–118.

Merlini, T., Morandini, M., 2013. On successive differentiations of the rotation tensor: an application to nonlinear beam elements. J. Mech. Mater. Struct. 8 (5), 305–340. doi:10.2140/jomms.2013.8.305.

Mielke, A., 1991. Hamiltonian and Lagrangian Flows on Center Manifolds with Applications to Elliptic Variational Problems. Lecture Notes in Mathematics, 1489. Springer Berlin / Heidelberg doi:10.1007/BFb0097544.

Morandini, M., Chierichetti, M., Mantegazza, P., 2010. Characteristic behavior of prismatic anisotropic beam via generalized eigenvectors. Int. J. Solids Struct. 47 (10), 1327–1337. doi:10.1016/j.ijsolstr.2010.01.017.

Nukala, P.K.V.V., White, D.W., 2004. A mixed finite element for three-dimensional nonlinear analysis of steel frames. Comput. Methods Appl. Mech. Eng. 193 (23), 2507–2545. doi:10.1016/j.cma.2004.01.029.

Papadopoulos, P., Lu, J., 1998. A general framework for the numerical solution of problems in finite elasto-plasticity. Comput. Methods Appl. Mech. Eng. 159 (1–2), 1–18.

Papadopoulos, P., Lu, J., 2001. On the formulation and numerical solution of problems in anisotropic finite plasticity. Comput. Methods Appl. Mech. Eng. 190 (37–38), 4889–4910. URL http://www.sciencedirect.com/science/article/B6V29-438BP1F-8/2/ea94ac851d0ea7c20ab0094a75a64ec2

Pietraszkiewicz, W., Eremeyev, V.A., 2009. On natural strain measures of the non–linear micropolar continuum. Int. J. Solids Struct. 46, 774–787.

Popescu, B., Hodges, D.H., 2000. On asymptotically correct Timoshenko-like anisotropic beam theory. Int. J. Solids Struct. 37 (3), 535–558. doi:10.1016/S0020-7683(99)00020-7.

Rezaiee-Pajand, M., Gharaei-Moghaddam, N., 2015. Analysis of 3d Timoshenko frames having geometrical and material nonlinearities. Int. J. Mech. Sci. 94–95, 140–155. doi:10.1016/j.ijmecsci.2015.02.014.

Rigobello, R., Breves Coda, H., Munaiar Neto, J., 2013. Inelastic analysis of steel frames with a solid-like finite element. J. Constr. Steel Res. 86, 140–152. doi:10.1016/j.jcsr.2013.03.023.

Romanova, N.M., Ustinov, Y.A., 2008. The Saint–Venant problem of the bending of a cylinder with helical anisotropy. J. Appl. Math. Mech. 72 (4), 481–488.

Simo, J.C., Hughes, T.J.R., 1998. Computational Inelasticity. Interdisciplinary Applied Mathematics, 7. Springer. URL http://www.springer.com/it/book/9780387975207

Wang, Y.-H., Nie, J.-G., Fan, J.-S., 2014. Fiber beam-column element for circular concrete filled steel tube under axial–flexure–torsion combined load. J. Constr. Steel Res. 95, 10–21. doi:10.1016/j.jcsr.2013.11.014.

Yu, W., Hodges, D.H., Ho, J.C., 2012. Variational asymptotic beam sectional analysis – an updated version. Int. J. Eng. Sci. 59 (0), 40–64. doi:10.1016/j.ijengsci.2012.03.006.

Zubov, L.M., 2006. The non-linear Saint–Venant problem of the torsion, stretching and bending of a naturally twisted rod. J. Appl. Math. Mech. 70 (2), 300–310.